Anisotropy in pair dispersion of inertial particles in turbulent channel flow

Enrico Pitton,[1] Cristian Marchioli,[1,2] Valentina Lavezzo,[3] Alfredo Soldati,[1,2] and Federico Toschi[3]
[1]*Centro Interdipartimentale di Fluidodinamica e Idraulica, Università degli Studi di Udine, 33100 Udine, Italy*
[2]*Department of Fluid Mechanics, CISM, 33100 Udine, Italy*
[3]*Department of Applied Physics, Technische Universiteit Eindhoven, 5600 MB Eindhoven, The Netherlands*

(Received 26 March 2012; accepted 13 June 2012; published online 27 July 2012)

The rate at which two particles separate in turbulent flows is of central importance to predict the inhomogeneities of particle spatial distribution and to characterize mixing. Pair separation is analyzed for the specific case of small, inertial particles in turbulent channel flow to examine the role of mean shear and small-scale turbulent velocity fluctuations. To this aim an Eulerian-Lagrangian approach based on pseudo-spectral direct numerical simulation (DNS) of fully developed gas-solid flow at shear Reynolds number $Re_\tau = 150$ is used. Pair separation statistics have been computed for particles with different inertia (and for inertialess tracers) released from different regions of the channel. Results confirm that shear-induced effects predominate when the pair separation distance becomes comparable to the largest scale of the flow. Results also reveal the fundamental role played by particles-turbulence interaction at the small scales in triggering separation during the initial stages of pair dispersion. These findings are discussed examining Lagrangian observables, including the mean square separation, which provide *prima facie* evidence that pair dispersion in non-homogeneous anisotropic turbulence has a *superdiffusive* nature and may generate non-Gaussian number density distributions of both particles and tracers. These features appear to persist even when the effects of shear dispersion are filtered out, and exhibit strong dependency on particle inertia. Application of present results is discussed in the context of modelling approaches for particle dispersion in wall-bounded turbulent flows.
 [http://dx.doi.org/10.1063/1.4737655]

I. INTRODUCTION

Suspensions of dust, droplets, and other finite-size particles advected by incompressible turbulent flows are commonly encountered in many natural and engineering flows.[1–8] Understanding how swarms of particles are moved by the underlying flow field is important in connection with dispersion, mixing and deposition phenomena. This connection clearly emerges in problems like air-quality control, dispersion of species in geophysical flows (e.g., clouds of contaminants in the atmosphere,[9] nutrients or drifters in the ocean,[10,11] and reacting flows, where characterization of particle concentration fluctuations is one of the key issues.[12,13] Fundamental knowledge of fluid-particles interaction and correct prediction of concentration fluctuations can be obtained examining the statistical properties of particle motion. Statistical properties richer in information seem those computed in the Lagrangian frame of reference, as underlined by Toschi and Bodenschatz[8] and by Salazar and Collins.[14] Lagrangian properties of particles in turbulence have been widely investigated in the context of two-particle dispersion problems, as demonstrated by the literature on the topic.[14] Of the many studies dealing with two-particle dispersion, most focus on the behavior of fluid tracers,[9,15,16] and consider flows where large-scale shear effects are not present.[16–18]

The objective of this paper is to provide a statistical characterization of pair dispersion for the more complicated case of inertial particles in turbulent shear flow. Compared to the case of

fluid tracers, inertial particles do not follow the flow exactly, and particle swarms exhibit complex, non-uniform clustered patterns which may be correlated to the topology of the flow.[2,19] Because of this inertia-induced preferential sampling, the particle velocity field is compressible even though the underlying fluid velocity field is incompressible. This causes fluctuations of particle concentration that alter the structure of particle patterns. This phenomenology has been demonstrated and discussed in many experimental works,[2,20] as well as numerical studies[21–28] and theoretical analyses.[17,29–31] From a modelling standpoint, reproducing accurately pair relative velocity and dispersion statistics is crucial to predict the effect of particle clustering on turbulent collisions and sedimentation.[17] In a series of recent papers,[32,33] Bec and co-workers characterized the relative dispersion of heavy point particles in homogeneous isotropic turbulence, focusing specifically on the scaling of particle velocity distribution at changing the degree of inertia in the different dispersive regimes (dissipative, inertial, and diffusive). A further complication is the presence of shear, which stretches the distance between particles and is expected to induce strong deviations from the usual diffusion laws. Shear effects on Lagrangian observables were investigated by Celani *et al.*,[34] who studied the dispersion of fluid tracers in turbulent isotropic flow with linear shear superposed. Relevant to the present paper is the finding that the range of validity of Richardson law for diffusion[35] is limited to timescales characteristic of the turbulent component of the flow whereas at longer timescales, characteristic of the shear, a different anisotropic behavior occurs.

To complement and extend current literature, we examine the dispersion of pairs of heavy particles in turbulent channel flow. In this case, the shear profile is a nonlinear function of the wall distance and its effects on particles are complicated by the interactions with a flow structure which is anisotropic along the wall-normal direction. This has an influence on the current framework used to model particle dispersion in sheared flows, since the model scales, as for instance the Lagrangian time scale of the fluid,[36] are strongly non-uniform across the channel.[37] Phenomena involving the effects of both shear and turbulent dispersion are currently modelled with approximated or *ad hoc* chosen scales.[36] Such modelling choices could be improved on the basis of statistical characterization of particle pairs coming from detailed numerical simulations.

The relative role of mean shear and turbulent fluctuations on dispersion is analyzed focusing on the mean square separation $\langle d^2(t)\rangle = \langle \mathbf{d}(t)\cdot\mathbf{d}(t)\rangle$, where $\mathbf{d}(t) = \mathbf{x}_p^{P_1}(t) - \mathbf{x}_p^{P_2}(t)$ represents the separation vector between two paired particles P_1 and P_2, $\mathbf{x}_p^i(t)$ represents the location of the ith particle at time t, and $\langle\cdot\rangle$ indicates an average over an ensemble of trajectory pairs. Statistics are organized in different families according to (i) the values of the particle Stokes number, St, defined as the particle response time normalized by a characteristic flow timescale; (ii) the location of pair release with respect to the walls; and (iii) the initial orientation of the separation vector. By doing so, we will find different time evolution for $\mathbf{d}(t)$ which depends on the properties of the particles (inertia, in particular) but also on flow characteristics—local mean shear, turbulent fluctuations and Lagrangian time scales—experienced by paired particles during the first stages of their motion. To our knowledge, there is no such database available for bounded flows: statistics presented in this paper might be particularly useful for validation of two-point Eulerian models, which are currently limited to homogeneous isotropic turbulence,[9,17] and for improving current physical understanding of multiple particle dispersion.[38]

The paper is organized as follows. In Sec. II, the equations of motion for both phases are briefly recalled and the numerical simulations are described. In Sec. III, qualitative phenomena and quantitative analysis of mean square separation of inertial particles and tracers are presented. To deepen this analysis, mean square separations are also evaluated by removing the shear dispersion effects.[39–41] This analysis is important in the context of the modelling strategies which are based on mimicking shear effects and turbulence dispersion as separate superimposed phenomena, given the large scale separation. Finally, in Sec. IV the main findings are summarized and recommendations for future research are given.

II. GOVERNING EQUATIONS AND NUMERICAL MODELLING

The reference geometry consists of two infinite flat parallel walls: the origin of the coordinate system is located at the center of the channel with the x, y, and z axes pointing in the streamwise,

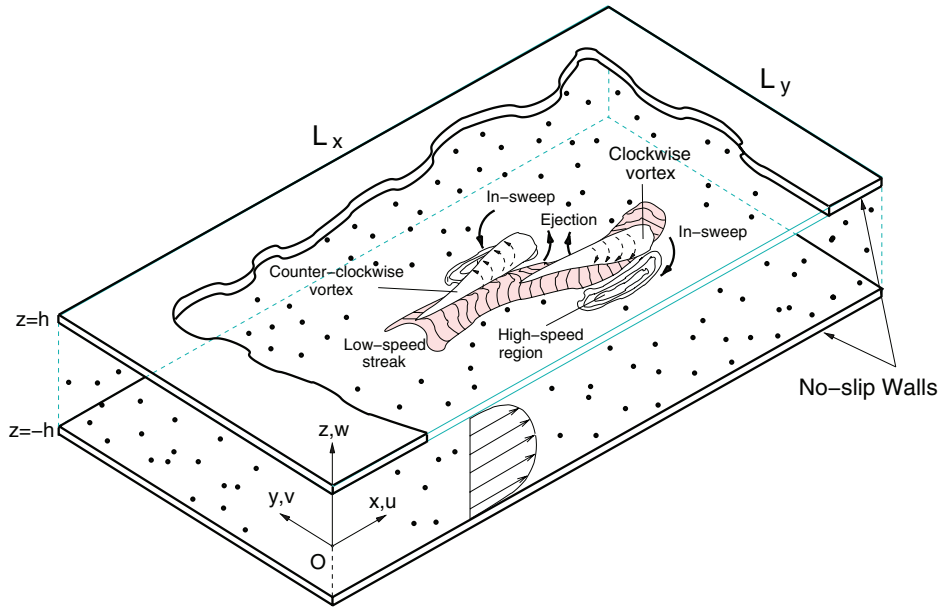

FIG. 1. Particle-laden turbulent gas flow in a channel: sketch of the computational domain and minimal schematics of near-wall turbulent coherent structures. Strong causal relationship links low-speed streaks to ejections generated by quasi-streamwise vortices, which also generate in-sweeps of high streamwise momentum fluid to the wall in the high velocity regions.

spanwise, and wall-normal directions, respectively (see Fig. 1). Periodic boundary conditions are imposed on the fluid velocity field in the homogeneous directions (x and y), no-slip boundary conditions are imposed at the walls ($z = -h$ and $z = h$ in Fig. 1). The size of the computational domain is $L_x \times L_y \times L_z = 4\pi h \times 2\pi h \times 2h$. We consider non-reactive, isothermal, and incompressible (low Mach number) flow and monodispersed particles. Calculations use dimensionless variables in wall units, indicated by the superscript $+$ hereinafter. Simulation parameters in the present study correspond to flow of air with density $\rho = 1.3$ kg m^{-3} and kinematic viscosity $\nu = 15.7 \times 10^{-6}$ m^2 s^{-1} moving at bulk velocity $u_b \simeq 1.65$ m s^{-1} in a 4 cm-high channel; in this frame particles have density $\rho_p = 10^3$ kg m^{-3} and diameters ranging from 45 to 230 μm (see Table I).

A. Equations for the fluid phase and flow solver

The governing balance equations for the fluid in dimensionless form read as

$$\frac{\partial u_i}{\partial x_i} = 0, \tag{1}$$

$$\frac{\partial u_i}{\partial t} = -u_j \frac{\partial u_i}{\partial x_j} + \frac{1}{Re_\tau} \frac{\partial^2 u_i}{\partial x_j{}^2} - \frac{\partial p}{\partial x_i} + \delta_{1,i}, \tag{2}$$

TABLE I. Relevant simulation parameters for the inertial particles: Stokes number (St), response time τ_p, dimensionless (d_p^+) and dimensional (d_p) diameter, and volume fraction (Φ_V).

St	τ_p(s)	d_p^+	d_p (μm)	Φ_V
5	5.660×10^{-3}	0.342	45.6	3.9×10^{-6}
25	2.832×10^{-2}	0.765	102	4.4×10^{-5}
125	1.415×10^{-1}	1.710	228	4.9×10^{-4}

where u_i is the ith component of the velocity vector, p is the fluctuating kinematic pressure, $\delta_{1,i}$ is the mean pressure gradient that drives the flow and $Re_\tau \equiv u_\tau h/\nu$ is the Reynolds number based on the shear (or friction) velocity, u_τ, and on the half channel height, h. The shear velocity is $u_\tau \equiv \sqrt{\tau_w/\rho}$, where τ_w is the mean shear stress at the wall. The superscript + is dropped from Eqs. (1) and (2) for ease of reading.

The flow solver used to perform the numerical simulations is based on a pseudo-spectral method that transforms the field variables into wave space to discretize the governing equations. In the homogeneous directions (x and y), all the quantities are expressed by Fourier expansions using k_x and k_y wavenumbers. In the wall-normal non-homogeneous direction, they are represented by Chebyshev polynomials. The solution, represented spectrally in all three flow directions, has the general form

$$\mathbf{u}(k_x, k_y, n) = \sum_{k_x} \sum_{k_x} \sum_{n} \hat{\mathbf{u}}(k_x, k_y, n) e^{i(k_x x + k_y y)} T_n(z), \tag{3}$$

in which $T_n(z) \equiv \cos[n \cdot \cos^{-1}(z/h)]$ is the nth order Chebyshev polynomial. By using the orthogonality property of $e^{i(k_x x + k_y y)}$, the equations for the Fourier coefficients $\hat{\mathbf{u}}(k_x, k_y, n)$ can be obtained. All the differential equations to be solved are of Helmholtz type with Dirichlet boundary conditions specified at the walls. Equations are time advanced using a two-level explicit Adams-Bashforth scheme for the nonlinear convection terms and an implicit Crank-Nicolson method for the diffusion terms. All calculations are carried out in wave space except for the nonlinear terms, which are computed in the physical space and then transformed back to wave space. This numerical scheme is standard for direct simulation of turbulence in domains of simple geometry, such as rectangular channels.[7]

B. Equations for the dispersed phase and Lagrangian particle tracking

In the Lagrangian framework, the motion of particles is described by a set of ordinary differential equations for particle position, $\mathbf{x}_p$, and velocity, $\mathbf{u}_p$. These equations in vector form read as

$$\frac{d\mathbf{x}_p}{dt} = \mathbf{u}_p, \tag{4}$$

$$\frac{d\mathbf{u}_p}{dt} = \frac{(\mathbf{u}_{@p} - \mathbf{u}_p)}{\tau_p} \left(1 + 0.15\, Re_p^{0.687}\right), \tag{5}$$

where $\mathbf{u}_{@p}$ is the fluid velocity at the particle position and $\tau_p \equiv \rho_p d_p^2/18\mu$ is the particle response time (d_p and μ being the diameter of the particle and the dynamic viscosity of the fluid, respectively). The Stokes drag coefficient is computed using a standard nonlinear correction[42] required when the particle Reynolds number, $Re_p = |\mathbf{u}_{@p} - \mathbf{u}_p| d_p/\nu$, does not remain small (i.e., sufficiently large inertia).

To calculate individual particle trajectories, a Lagrangian tracking routine is coupled to the DNS flow solver. The routine solves for Eqs. (4) and (5) under the following assumptions: (i) particles are pointwise, non-rotating rigid spheres (point-particle approach) and (ii) particles are injected into the flow at concentration low enough to consider dilute system conditions: the effect of particles on the fluid and inter-particle collisions are neglected. Equations of particle motion are advanced in time by a 4th-order Runge-Kutta scheme: at the beginning, particles are randomly distributed over the computational domain and their initial velocity is set equal to that of the fluid at their location. Fluid velocity interpolation is performed by 6th-order Lagrangian polynomials (near the wall, the interpolation scheme switches to one-sided). The timestep for tracking heavy particles is $\delta t^+ = 0.45$, corresponding to about one tenth of the non-dimensional response time of the smallest particle tracked ($d_p = 45.6$ μm, see Table I) and ensuring adequate description of particle dynamics.[43] Periodic boundary conditions are imposed on particles moving outside the computational domain in the homogeneous directions. Perfectly elastic collisions at the smooth walls are assumed when the particle center is at a distance lower than one particle radius from the wall.

For the purposes of the present study, we decided to keep the simulation setting as simplified as possible to minimize the degrees of freedom. Inclusion of additional forces such as gravity and lift[44,45] or incorporation of two-way coupling effects would just add quantitative corrections within the range of parameters examined—particle dimension (see Table I for details), density, and concentration—and would not modify the quality of the model.[24]

C. Simulation parameters

Results presented in this paper are relative to a value of the shear Reynolds number $Re_\tau = 150$ corresponding to a shear velocity $u_\tau = 0.11775$ m s^{-1}. The average (bulk) Reynolds number is $Re_b \equiv u_b h/\nu = 2100$. The size of the computational domain in wall units is $L_x^+ \times L_y^+ \times L_z^+ = 1885 \times 942 \times 300$. The computational domain was discretized in physical space with $128 \times 128 \times 129$ grid points (128×128 Fourier modes and 129 Chebyshev coefficients in the wave space). Flow field data are taken from the same repository used for the benchmark test described in Marchioli *et al.*[43]

Samples of $n_p = 4.2 \times 10^6$ particles characterized by different response times were considered. The response time is made dimensionless using wall variables, and the Stokes number is thus obtained as $St \equiv \tau_p^+ = \tau_p/\tau_f$ where $\tau_f \equiv \nu/u_\tau^2$ is the viscous timescale of the flow. This characteristic time scale supplies a measure of the time available for eddy-particle interaction. Table I summarizes the complete set of parameters relevant to the simulations of particle pair dispersion. We remark that the characteristic timescale of the flow changes depending on the specific value of the shear Reynolds number, namely on the specific value of the shear velocity. In the present case, $\tau_f = 1.13 \times 10^{-3}$ s.

D. Initial pair arrangement

The initial distribution of position, velocity, and orientation of particle pairs is an important issue when looking at the relative effects of mean shear and turbulence fluctuations on dispersion in wall-bounded shear flow, because small differences in the initial conditions can determine large differences in the evolution of statistics. This is due to anisotropy and non-homogeneity, which are particularly exhibited by the dissipative scales, as demonstrated by the wall-normal behavior of the Kolmogorov length scale, $\overline{\eta}_K = \left(\nu^3/\overline{\epsilon}\right)^{1/4}$ with $\overline{\epsilon}$ the mean dissipation rate, shown in Fig. 2 (the overline indicates average over the homogeneous directions and in time). This feature has an impact on the overall dispersion process because the same separation distance might correspond to different dispersion regimes depending on the local value of $\overline{\eta}_K$. In addition, anisotropy changes the shear

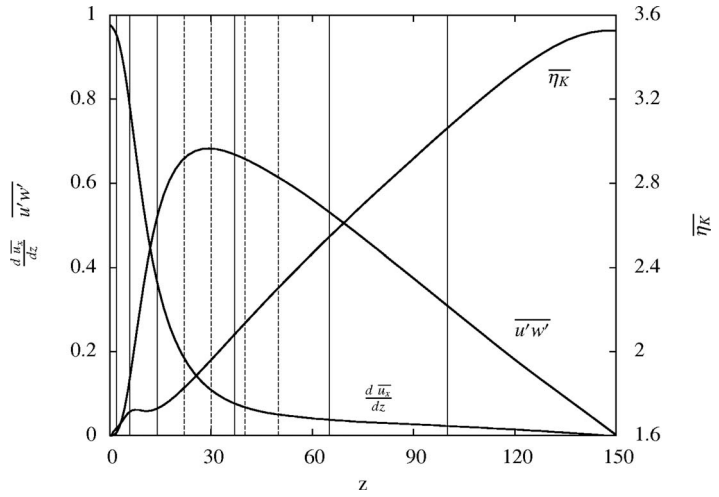

FIG. 2. Wall-normal behavior of (a) dissipative Kolmogorov scale, $\overline{\eta}_K$; mean shear, $\mathrm{d}\overline{u}_x/\mathrm{d}z$; and Reynolds stress, $\overline{u'w'}$. Wall-normal locations of pair release are indicated by horizontal solid lines, dashed lines indicate additional pair release locations that were considered for tracers only.

characteristics and the Reynolds stresses acting on particles, also shown in Fig. 2. All quantities in this figure are in non-dimensional form and superscript + has been suppressed to alleviate notation: shear is quantified via the mean streamwise velocity gradient $\mathrm{d}\overline{u}_x/\mathrm{d}z$ and Reynolds stress by its $\overline{u'w'}$ component. To emphasize the effect produced by such turbulence characteristics on pair dispersion, we identified suitably chosen locations of release for the particle pairs. At the beginning of each tracking, large swarms of particle pairs were positioned in wall-parallel planes located at increasing distances from the wall as shown in Fig. 2: seven release planes (located at $z^+ = 2$, 6, 14, 37, 65, 100, and 150, respectively) were chosen for inertial particles, whereas four additional release planes were chosen only for tracer particles across the $z^+ = 37$ release plane, which corresponds to the location of maximum Reynolds stress. We wish to remark here that the choice of the $z^+ = 37$ release plane was made because of the influence that Reynolds stress has on downstream square separation, $\langle d_x^2(t)\rangle$. Following Deardorff and Peskin,[46] one can write

$$\langle d_x^2(t)\rangle = 2\left[\langle x'^2(t)\rangle - \langle x'^{P_1}_p(t)\cdot x'^{P_2}_p(t)\rangle\right] + 2\langle[x'^{P_1}_p(t) - x'^{P_2}_p(t)]\cdot[\bar{x}^{P_1}_p(t) - \bar{x}^{P_2}_p(t)]\rangle + \langle[\bar{x}^{P_1}_p(t) - \bar{x}^{P_2}_p(t)]^2\rangle, \quad (6)$$

where $\langle x'^2(t)\rangle = [\langle x'^{P_1}_p(t)\cdot x'^{P_1}_p(t)\rangle + \langle x'^{P_2}_p(t)\cdot x'^{P_2}_p(t)\rangle]/2$, $x'^i_p = x^i_p(t) - \bar{x}^i_p(t)$, $\bar{x}^i_p(t) = \bar{x}^i_p(0) + \int_0^t u_x(z^i_p)\mathrm{d}\tau$ is the mean downstream displacement with $i = P_1$, P_2, and $\langle x'^{P_1}_p(t)\cdot x'^{P_2}_p(t)\rangle$ is the two-particle distance correlation. In Eq. (6), the second term on the right-hand side represents the combined influence of Reynolds stress and mean shear, and the last term represents the direct effect of mean shear alone.

To categorize further the statistics, pairs were arranged on each release plane according to three different initial orientations obtained putting the two paired particles virtually in touch, with their centers of mass (where all forces are exerted under the pointwise modelling approximation) at one particle diameter distance along either the streamwise, the spanwise or the wall-normal direction. When particle diameter is changed, also the initial pair separation distance, d_0, is changed. We remark however that even for the larger particles d_0 is smaller than the Kolmogorov lengthscale. By doing so, we expose particles to different levels of small-scale turbulent fluctuations (which are particularly intermittent) and to different shear-induced velocity gradients making it possible to explore their mutual influence on relative Lagrangian dispersion properties. This is especially important at early times, when the Eulerian structure of the flow has a strong effect on two-particle statistics. The Lagrangian approach is chosen here because it addresses naturally transport-related issues by tracing the trajectories of individual particles, like those shown in Fig. 3 for the case of two

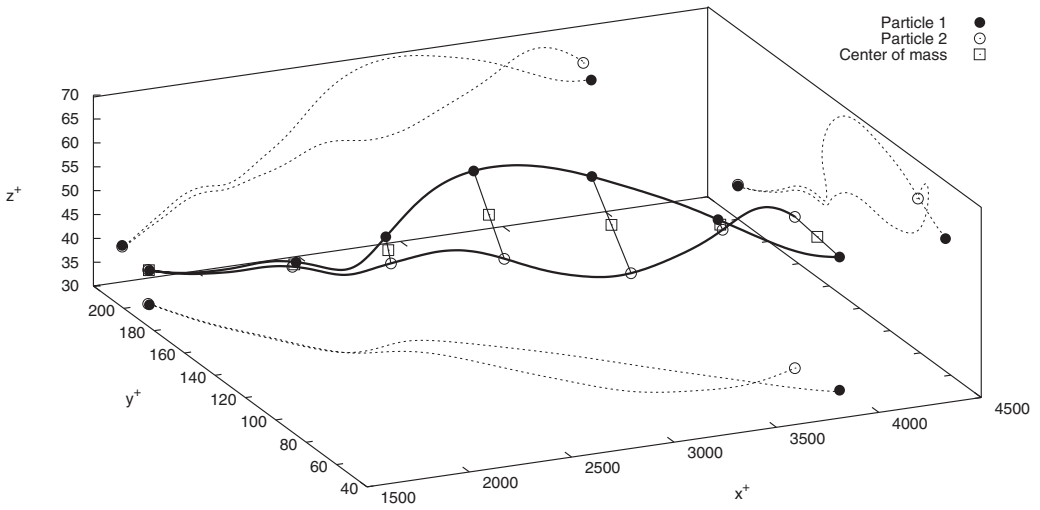

FIG. 3. Trajectories of two heavy $St = 25$ particles released at $z^+ = 37$ with initial spanwise separation $d_0{}^+ = 0.76$. The position of each particle is shown together with the center of mass of the particle pair (□) and the three-dimensional separation distance vector (−). Projection of trajectories on the different cross-sectional planes are also visualized (dashed lines).

paired $St = 25$ particles. The statistical repository gathered in this work for inertial particles covers a total of 63 cases (3 Stokes number families of $\mathcal{N}_p = 10^5$ pairs tracked on $N_{pl} = 7$ release planes with $N_{or} = 3$ initial orientations), complemented by 33 cases for tracers (1 Stokes number family of $\mathcal{N}_p = 10^5$ pairs tracked on 11 release planes with 3 initial orientations). Note that $n_p = 2\mathcal{N}_p N_{pl} N_{or}$. We remark here that the number of pairs per release plane, $\mathcal{N}_p$, was chosen to ensure converged statistics based on the evaluation of the normalized mean square error over $\mathcal{N}_s$ tracking tests performed using $n_p^{min} = 2\mathcal{N}_p/\mathcal{N}_s$ individual particles:

$$\sigma_u(t) = \frac{1}{\mathcal{N}_s} \sum_{i=1}^{\mathcal{N}_s} \frac{\left[\tilde{d}_i(t) - \mathcal{D}(t)\right]^2}{\left[\mathcal{D}(t)\right]^2}, \tag{7}$$

where, given the separation $d_{i,j}(t)$ of the jth pair in the ith tracking test, we defined $\tilde{d}_i(t) = \frac{2}{\mathbf{n}_p^{\min}} \sum_{j=1}^{\mathbf{n}_{p/2}^{\min}} d_{i,j}(t)$, and $\mathcal{D}(t) = \frac{1}{N_s} \sum_{i=1}^{\mathcal{N}_s} \tilde{d}_i(t)$. For $\mathcal{N}_s = 4$ it was found that $\sigma_u \leq 1\%$ for $\mathcal{N}_p = 10^5$.

III. RESULTS AND DISCUSSION

In this section, we provide a detailed quantitative analysis of the separation process based on the evaluation of Lagrangian observables, first focusing on time-dependent square separation statistics and then discussing conditional number density distribution statistics. The inclusion of conditional statistics is crucial to describe pair dispersion in consistent physical terms, and the reason is associated with the intermittent character of separation. In fact, square separation statistics were computed performing fixed-time ensemble averages of the particles relative displacement. However, as already pointed out in previous works dealing with isotropic turbulence,[16,47,48] particle pairs are not expected to enter a certain dispersion regime at the same time, and the arrival time of the particle separation to a certain threshold (i.e., the exit time from a certain dispersion regime) can vary significantly. This is associated with the formation of a broad distribution of separations and results in "contamination" of the statistics, especially those based on fixed-time averaging, by both slowly separating pairs (which remain close together) and rapidly separating pairs (which approach the integral scales). Paired particles separating with widely varying growth rates are observed also in the channel flow configuration considered here, as demonstrated by Fig. 4. This figure provides a qualitative visualization of few sample trajectories, projected in the longitudinal $x^+ - z^+$ plane, for the two limiting cases of particles travelling together for a long time span (represented with empty circles) and of particles quickly parting their paths (represented with filled circles). In particular, Fig. 4(a) refers to two pairs A and B released from the center of the channel ($z^+ = 150$): pair B does not separate and remains confined in the core flow while travelling downstream; pair A separates as the two particles are brought in the proximity of the wall by turbulence and become exposed to increasing streamwise velocity differences. Eventually, particle A_1 gets trapped in the viscous sublayer and deposits whereas particle A_2 is able to escape the near-wall region. Fig. 4(b) shows four pairs released near the wall ($z^+ = 2$), and selected because of their "symptomatic" behavior: both particles pertaining to pairs C and E remain trapped very close to the wall and do not separate; pairs D and F undergo strong separation due to the large velocity difference existing between the particle that remains trapped at the wall (e.g., D_1 and F_1) and the particle that escapes the near-wall region (e.g., D_2 and F_2). It is worth noting that, in both situations, particle dynamics must be analyzed considering that paired particles with equal response time may react to local flow perturbations whose timescale changes significantly with the distance from the wall. This is exemplified in Fig. 4(c), where the wall-normal behavior of the *scale-dependent* Stokes number, St_K, is shown. This quantity is defined as $St_K = \tau_p/\tau_K$, τ_K being the Kolmogorov timescale. For the present channel flow configuration, the non-dimensional Kolmogorov timescale, $\tau_K^+ = \tau_K/\tau_f$ ranges from 2 wall units at the wall to 13 wall units at the channel centerline.[37] Hence, the values of St_K for the $St = 25$ particles shown in Fig. 4 range from $St_K(z^+ = 0 \text{ or } 300) \simeq 10$ (e.g., for particles A_1, D_1, and F_1) to $St_K(z^+ = 150) \simeq 2$ (e.g., for particles B and D_2).

The behavior just described is a macroscopic manifestation of the pair dispersion process, which owes its complexity to the irregularity and variability of particle paths. It is also an indication

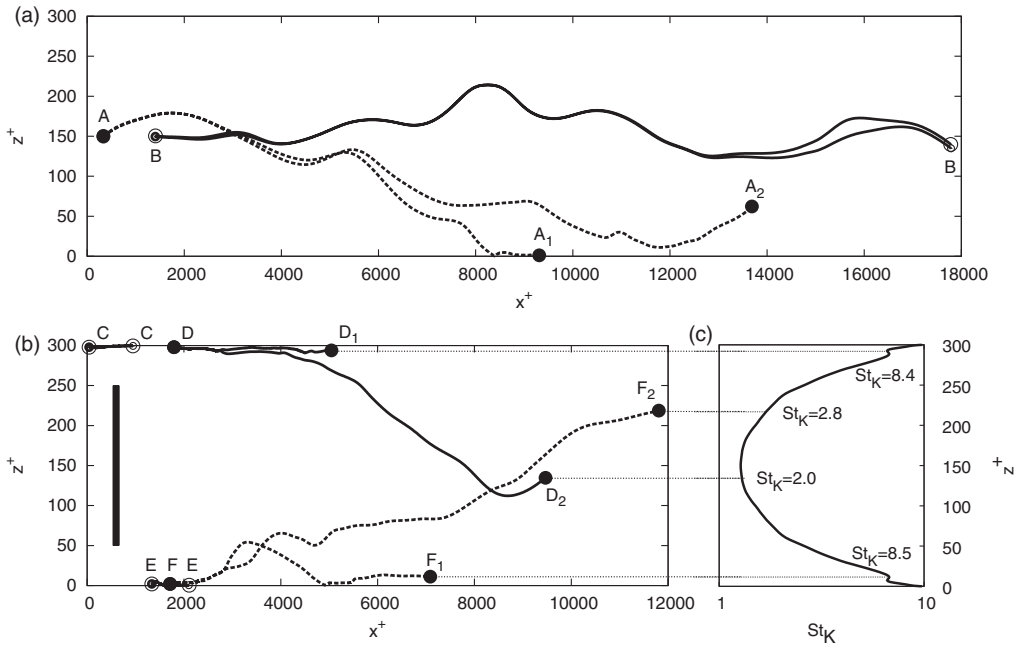

FIG. 4. Two-dimensional projections of six $St = 25$ particle pairs trajectories in the longitudinal $x^+ - z^+$ plane. Panel (a) refers to particle pairs released in the center of the channel ($z_0{}^+ = 150$) and panel (b) refers to particle pairs released close to the wall ($z_0{}^+ = 2$). The vertical bar in panel (b) provides an indication of the horizontal-to-vertical scaling of the 2D view: the minor (resp. major) side of the bar covers 200 wall units in x^+ (resp. z^+). Panel (c) shows the wall-normal behavior of the Stokes number St_K based on the Kolmogorov time scale, τ_K. Values of St_K for few sample particles shown in panel (b) are indicated.

that different dispersion regimes may overlap due to particle separation being influenced more by characteristic lengths of the velocity field than by characteristics times,[47] and generate possible statistical bias. Hence the need to complement fixed-time statistics with fixed-scale statistics.

A. Mean-square separation statistics

We start our statistical analysis by examining the time behavior of the mean square separation, $\langle d^2(t)\rangle$. Statistics for both tracers and inertial particles, obtained considering different release planes and different initial orientations, are compared directly to disentangle the effects due to mean shear and turbulent fluctuations at varying inertia. To this purpose, the extent ΔT of the time window over which statistics were gathered (and ensemble average performed) is expressed in terms of number of *crossingtimes*, τ_{ct}, one crossing time being the time taken by a fluid particle travelling with the centerline fluid velocity u_{cl} to cover one channel length L_x along the streamwise direction. In the present simulations, the dimensionless values of τ_{ct} and ΔT are

$$\tau_{ct}^+ = \frac{L_x^+}{u_{cl}^+} = \frac{1885}{17.8} \simeq 106 \rightarrow \Delta T^+ = 900 = 8.5\,\tau_{ct}^+. \tag{8}$$

In this work, ensemble averages (represented by brackets) were performed over all particles belonging to a given Stokes number family, regardless of particles instantaneous location. The corresponding Lagrangian statistics will thus owe their evolution to the specific dispersion dynamics of that family, and will most likely incorporate information from particles that are positioned in regions of the flow with significantly different characteristics. This aspect is of particular importance in non-homogeneous anisotropic turbulent flows (and more so in the channel flow considered in this study), where the velocity field is intermittent and not short correlated in time. In Fig. 5, we show the time evolution of particle spatial distribution in the longitudinal $x^+ - z^+$ plane for the family of inertial particles with $St = 25$ released from the $z^+ = 150$ plane with initial separation in the wall-normal direction. Note that, for ease of discussion, the $St = 25$ particles will be considered

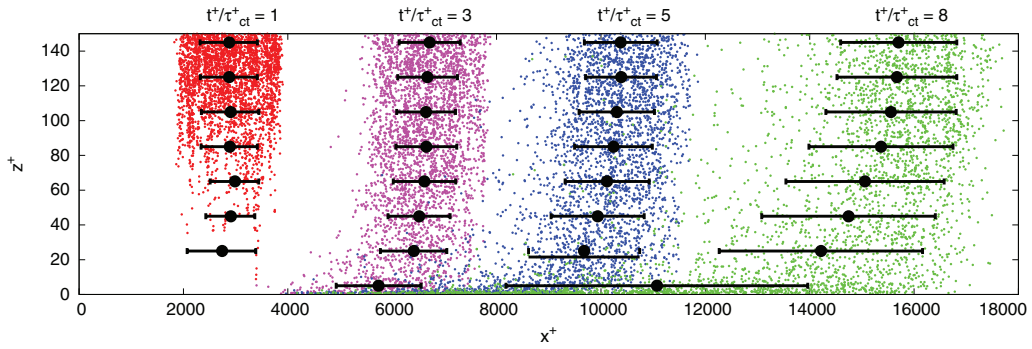

FIG. 5. Instantaneous $St = 25$ particle distribution at different times ($t^+/\tau^+_{ct} = 1$, 3, 5, and 8). For ease of visualization only one half of the channel is shown. Black dots (•) indicate the average streamwise position, $\langle \mathcal{X} \rangle$, of the particle swarm at a given distance z^+ from the wall, errorbars (⊢——⊣) quantify the spread around $\langle \mathcal{X} \rangle$ corresponding to the rms value, $RMS(\mathcal{X})$.

hereinafter as reference for comparison against tracers. Fig. 5 visualizes clearly how the swarm of particles spreads towards the wall as time increases. After one crossing time, all particles have covered one channel length but only a minor proportion has travelled more than half of its way to the wall. This behavior is consistent with the structure of both the mean and the fluctuating velocity fields in this flow: at early stages particles are mainly advected downstream as a result of injection in a region of high streamwise velocity but low mean shear, whereas cross-stream motions are controlled by turbulent fluctuations. Eventually, a large proportion of particles approaches the wall convected along the gradients of turbulence intensity and accumulates in the near-wall region where advection due to mean velocity decreases and relative dispersion due to mean shear reaches a maximum, as it becomes clear towards the end of the tracking (see, e.g., particle distribution at $t^+ \simeq 8\tau^+_{ct}$).

In an effort to quantify the qualitative observations drawn from Figs. 4 and 5, in Figs. 6 and 7 we show the time evolution of the mean square dispersion $\langle d^2(t) \rangle$ for tracers and for inertial ($St = 25$) particles, respectively. A combined analysis of these two figures is sufficient to highlight several important features of the pair dispersion process. To allow direct comparison of results, the initial pair separation d_0 was chosen to be the same for both tracers and particles. First, the effect of the flow field anisotropy emerges clearly after comparison of $\langle d^2(t) \rangle$ profiles for inertia-less tracer pairs characterized by different release planes and initial pair orientations. When released in the near-wall region (Figs. 6(a) and 6(b)), pairs initially displaced along the wall-normal direction separate at a much faster rate[49] than those initially displaced along wall-parallel directions (Fig. 6(a)). This behavior is of course due to the action of the high local fluid velocity gradients which readily stretch cross-stream oriented pairs along the streamwise direction thus decorrelating the relative velocity of tracers. At large times, relative dispersion of tracers released near the wall seems to be controlled by such shear-induced separation mechanism regardless of the initial orientation. This is demonstrated in Fig. 6(b), where it is shown that $\langle d^2(t) \rangle$ (open squares) has its largest component in the streamwise direction (solid line) and the smallest in the wall-normal direction (dashed-dotted line) also for pairs with initial separation vector oriented in the streamwise direction. As the release plane is shifted farther away from the wall (Figs. 6(c)–6(f)) initial pair orientation becomes less important in determining the overall relative dispersion: in the center of the channel, in particular, changes in orientation produce almost no difference in the evolution of $\langle d^2(t) \rangle$ (Fig. 6(e)).

A further important feature highlighted by Figs. 6(b), 6(d), and 6(f) is how the dispersion characteristics in the three-dimensional domain space as well as in the streamwise, spanwise and wall-normal coordinate directions differ as a result of non-uniform shear. These characteristics have been studied previously by Shen and Yeung[50] yet for fluid particles in homogeneous—unbounded—turbulent flow with uniform shear. Present results (only those relative to initial pair separation aligned with the mean flow are shown for brevity) indicate that relative separation is weaker when paired tracers are released near the wall (e.g., $\langle d^2(t) \rangle \simeq \mathcal{O}(10^0)$ after one crossing time in Fig. 6(b)) while it is enhanced when paired tracers are released in the $z^+ = 37$ plane, which corresponds to the region of

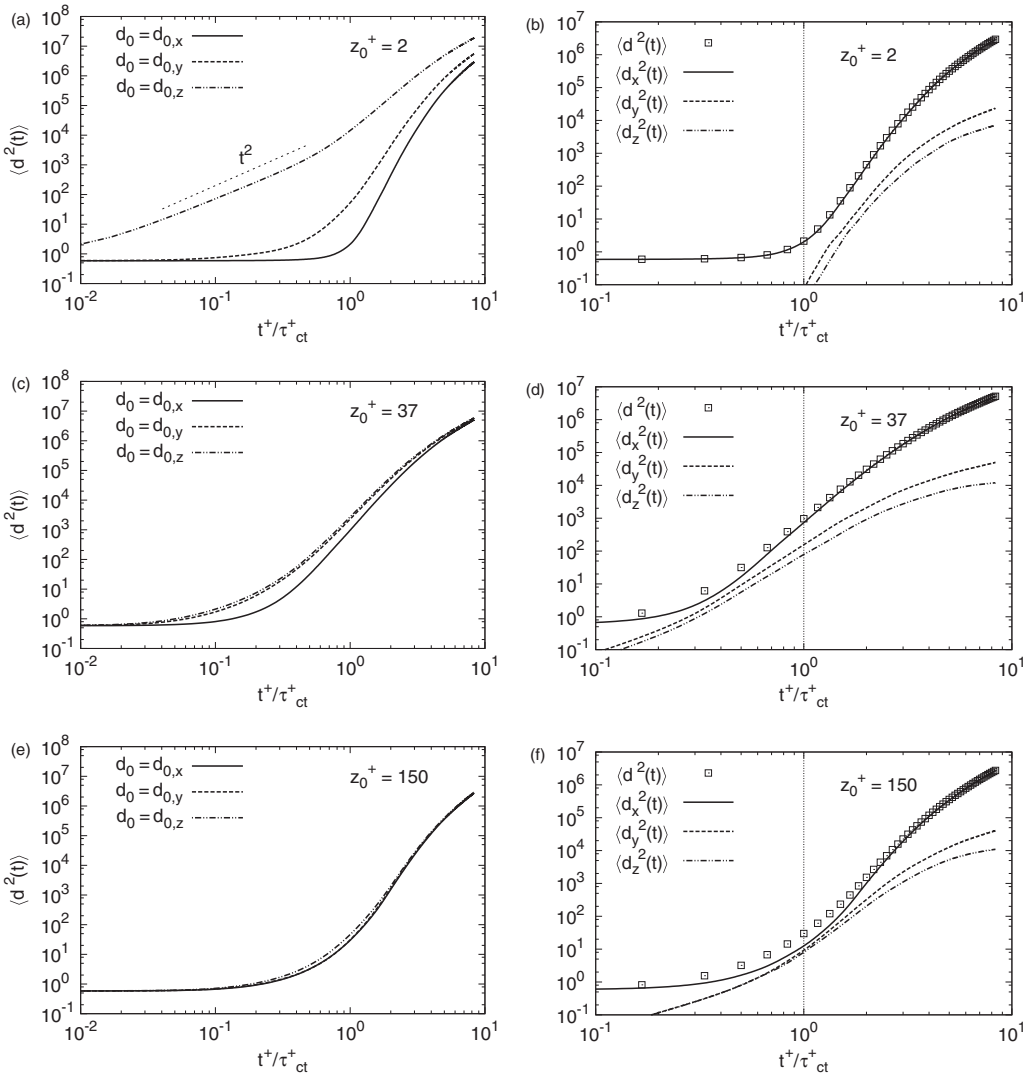

FIG. 6. Time evolution of the mean-square separation, $\langle d^2(t)\rangle$, for tracer pairs. Left panels: Behavior of $\langle d^2(t)\rangle$ for pairs with initial separation vector oriented in the streamwise ($d_0 = d_{0,x}$), spanwise ($d_0 = d_{0,y}$), and wall-normal ($d_0 = d_{0,z}$) directions, respectively. Right panels: Behavior of the components of $\langle d^2(t)\rangle$ for pairs with initial separation vector oriented in the streamwise direction. Statistics are shown for three release planes: $z_0{}^+ = 2$ (a) and (b), $z_0{}^+ = 37$ (c) and (d), and $z_0{}^+ = 150$ (e) and (f).

maximum shear stress (e.g., $\langle d^2(t)\rangle \simeq \mathcal{O}(10^3)$ after one crossing time in Fig. 6(d)). The trend is non monotonic since relative separation decreases again when the release plane is located in the channel centerline (e.g., $\langle d^2(t)\rangle \simeq \mathcal{O}(10^1)$ after one crossing time in Fig. 6(f)). If the square separation vector is projected onto the Eulerian coordinates, it can be observed that the streamwise component $\langle d_x^2(t)\rangle$ (solid line) is always dominant for large times, when it becomes roughly two orders of magnitude larger than both the spanwise ($\langle d_y^2(t)\rangle$, dashed line) and the wall-normal ($\langle d_z^2(t)\rangle$, dashed-dotted line) components. Interestingly, however, such large magnitude difference in the $\langle d^2(t)\rangle$ components is not observed for short times (e.g., $t^+ = \tau_{ct}^+$) when tracers are released in the channel centerline (Fig. 6(f)). This observation suggests that relative dispersion in this region is dominated by the small-scale turbulent fluctuations of the fluid velocity field up to times when the pair distance reaches scales large enough for the separation dynamics to be again dominated by mean shear. We also remark here that the wall-normal component of the mean square separation, $\langle d_z^2(t)\rangle$, cannot grow unbounded being limited by obvious geometric constraints: our results indicate that $\langle d_z^2(t)\rangle \simeq 10^4$ at the end of the tracking, namely that $\langle d_z(t)\rangle \simeq 10^2$. This asymptotic value is significantly smaller than the

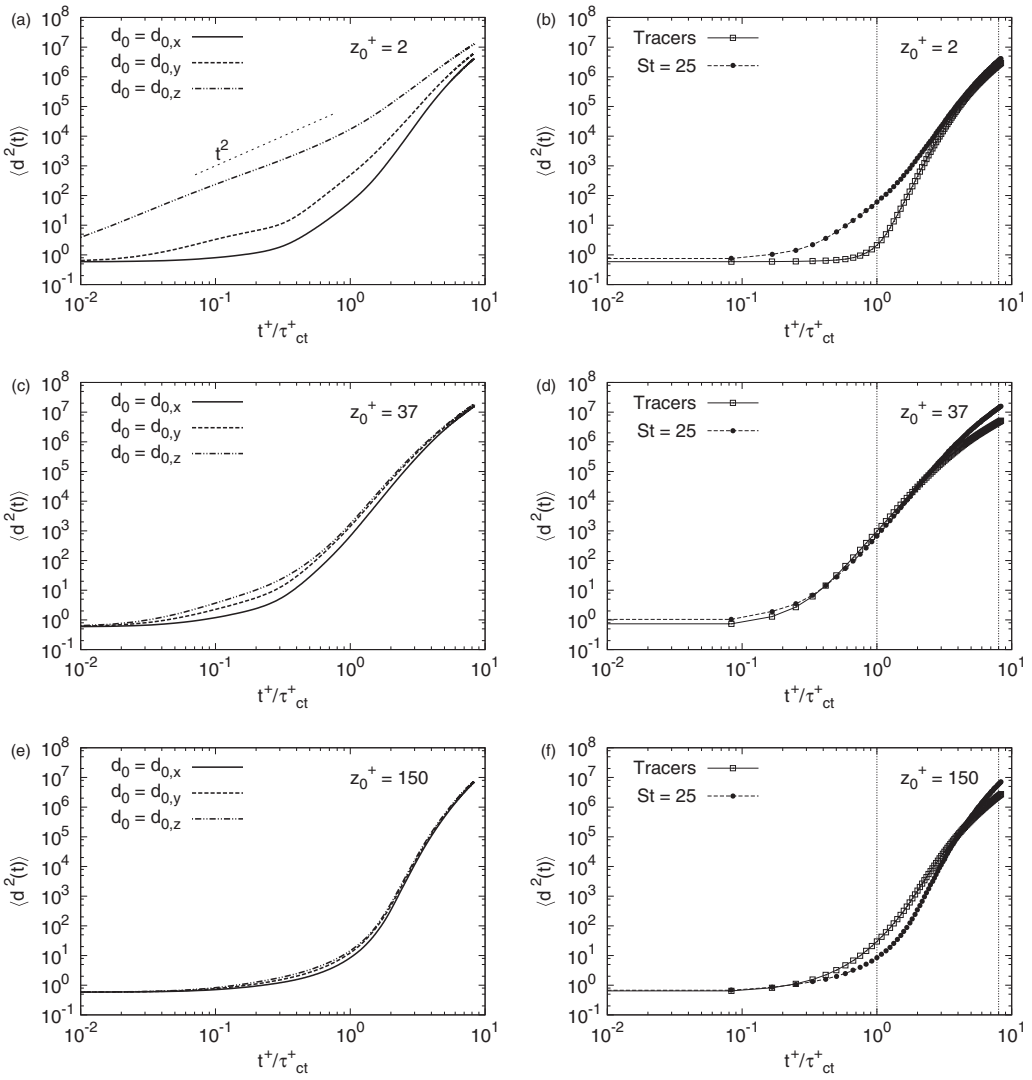

FIG. 7. Time evolution of the mean-square separation for inertial ($St = 25$) particle pairs. Left panels: Behavior of $\langle d^2(t) \rangle$ for pairs with initial separation vector oriented in the streamwise ($d_0 = d_{0,x}$), spanwise ($d_0 = d_{0,y}$), and wall-normal ($d_0 = d_{0,z}$) directions, respectively. Right panels: Comparison between time-evolving $\langle d^2(t) \rangle$ for tracers and for inertial ($St = 25$) particles for pairs with initial separation vector oriented in the streamwise direction. Statistics are shown for three release planes: $z_0^+ = 2$ (a) and (b), $z_0^+ = 37$ (c) and (d), and $z_0^+ = 150$ (e) and (f).

maximum possible value for $\langle d_z(t) \rangle$ ($\langle d_z^{max}(t) \rangle = 2 \cdot Re_\tau = 300$) and seems to suggest that the final spatial distribution attained by paired tracers is preferentially confined within one half of the channel, as will be discussed in Sec. III C.

In Fig. 7 we contrast the time evolution of $\langle d^2(t) \rangle$ obtained for heavy particles with that previously discussed for tracers to highlight additional effects on pair dispersion due solely to inertia. Figs. 7(a), 7(c), and 7(d) demonstrate that the effect of the initial pair orientation on the time evolution of $\langle d^2(t) \rangle$ shares several qualitative features with that already discussed for tracers (Fig. 6). Similarly to tracers, we notice that paired particles released very near the wall separate much faster if initially oriented in the mean velocity gradient direction (Fig. 7(a)), and that the rate at which they are swept apart from each other becomes more and more independent of the initial pair orientation as the selected release plane approaches the channel centerline (Figs. 7(c) and 7(e)). The tendency to achieve higher relative separation when pairs are released in the region of maximum shear stress is also maintained.

However, some important quantitative differences arise which can be evaluated examining Figs. 7(b), 7(d), and 7(f). In these figures, we compare directly the profiles of $\langle d^2(t)\rangle$ obtained for tracers and for inertial particles, conditioned on the location of pairs release. Error bars due to statistical fluctuations are of the order of the symbol size. When pairs are injected into the flow near the wall (Fig. 7(b)), inertial particles appear to move apart at a much faster rate than tracers during the initial stages of separation, and until the long-period effect of shear on downstream dispersion becomes dominant. A systematic increase in the value of $\langle d^2(t)\rangle$ is observed for $t^+ \geq 0.1\tau_{ct}^+$ in the case of particles, and only for $t^+ \geq 0.5\tau_{ct}^+$ in the case of tracers; asymptotically, profiles collapse onto each other. When pairs are injected in the region of maximum shear stress (Fig. 7(d)), there is virtually no difference in the evolution of $\langle d^2(t)\rangle$ (namely there is no effect due to particle inertia) up to two crossing times: then particle separation is faster than tracer separation. Finally, when pairs are injected near the channel centerline (Fig. 7(f)), trend reverses and a time lag interval is observed in which tracers separation proceeds faster than particles. The departure of inertial particles from tracers behavior is remarkable, covers roughly the first three crossing times and is made clearly evident by virtue of the small initial distance imposed to paired tracers/particles (note that d_0 is always smaller than the local Kolmogorov length scale). Similar findings have been reported in previous studies[32,51] yet for homogeneous isotropic turbulent flow. For this flow instance, the observed differences from the tracer behavior were attributed to the occurrence of caustics[31,52] which give singular contributions to the particle velocity increments inside the viscous range thus making the particle velocity difference with respect to the underlying fluid large.[32] More specifically, it was found that turbulent dispersion of heavy particles is governed by two temporal regimes: the first is dominated by small-scale caustics in the particle velocity statistics, the second starts once particle velocity has relaxed towards fluid velocity and the usual Richardson dispersion is observed for both particles and tracers.[32]

Counter to intuition, present results seem to indicate that the behavior just mentioned is macroscopically recovered when pairs are released in the near-wall region, where anisotropy and flow inhomogeneities dominate, rather than in the channel centerline, where turbulence becomes more homogeneous and isotropic. A possible explanation to this finding is related to the well-known phenomena of inertial particle segregation and preferential concentration.[2,21,24] It has been long established that heavy particles in low Reynolds turbulence are governed by fluid strain, namely centrifuged out of the turbulent eddies and accumulated in regions of low vorticity and high strain rate. In the near-wall region, the centrifuging phenomenology implies that particles are preferentially displaced in the cross-stream plane by the turbulent vortical structures which populate this region and generate areas of high streamwise vorticity alternated to areas of high cross-stream strain.[53] Due to such selective particles-turbulence interaction, pairs can be readily transported along the spanwise and, most importantly, along the wall-normal directions by vortices. During this motion, the residual turbulent velocity fluctuations near the wall (here comparable to the mean velocity) perturb continuously pairs separation distance, which then grows in its wall-normal and spanwise components more than in its streamwise component (see Fig. 7(a)). Increased cross-stream separation, in turn, induces significant particle pair velocity differences $\delta\mathbf{u}_p$ (Ref. 54) in the mean gradient direction, which ultimately trigger streamwise separation. This chain of events is not experienced by tracers which do not undergo vortical centrifugation because of their ability to follow exactly the flow. Hence, tracer pair separation cannot be boosted by this mechanism within the initial temporal regime dominated by inertial effects and small-scale turbulent fluctuations. After such a transient, the relative separation dynamics forgets the initial condition and tracers separate explosively (see Fig. 7(b)) with a power-law behavior which however does not recover in a clear manner the Richardson prediction. Away from the wall, the three components of the fluctuating vorticity are identical[53] and there is no preferential direction for particles sweeping by turbulent structures, as demonstrated by Fig. 7(e). In addition, the shear rate is small and the streamwise fluid velocity becomes predominant compared to velocity fluctuations. Under these conditions, small-scale turbulence is not able to induce significant velocity differences $\delta\mathbf{u}_p$ (at least sufficient to trigger from the very beginning streamwise separation of pairs) and preferential concentration has a sort of *damping effect* on relative dispersion of inertial particles. Again, these effects are not felt by tracers, which maintain their capability to diffuse faster upon injection into the flow. To put in a correct perspective the evaluation of pair response to the

underlying turbulence, it must be recalled that particle inertia is a scale-dependent quantity in our problem (see discussion of Fig. 4).

A final remark on Figs. 6 and 7 is that it is not possible to either identify a clear Richardson scaling or distinguish between Richardson and Batchelor scaling from these figures. This limitation is quite common to numerical studies based on direct numerical simulation[16,55] but was also encountered in experiments,[56,57] and arises because the flow Reynolds number is not large enough to provide the separation of scales that is required to observe a wide enough inertial range. It is thus believed that a broad crossover from the dissipation regime (in which separation grows exponentially) to the diffusion regime exists that hides the intermediate inertial range regime.[55] An alternative explanation was proposed recently by Rast and Pinton[18] who hypothesize that Richardson scaling is not prevented by a lack of inertial range dynamics. Rather it is blurred by intermittent dynamics, due to successive trappings of particles by turbulent coherent structures, which generate a broad distribution of delay times, one delay time being the time needed for the distance between a particle pair to increase significantly (by a factor of 2, for instance). According to Rast and Pinton,[18] the averaging over these delays dominates the observed $\langle d^2(t)\rangle$ behavior.

B. Single-particle PDFs

In Sec. III A, we have demonstrated how the flow stretches the distances between particles along the shear, altering the usual diffusion law. We have also shown that this process appears to be governed by two distinct time regimes for separation: an inertia-modulated regime, in which separation is triggered by small-scale interactions between particles and turbulence; and a subsequent shear-dominated regime, in which long-term separation is governed by mean shear. In spite of all the useful information provided by the analysis of the time-evolving mean square pair separation, there are still some unanswered questions concerning the interplay between flow field characteristics (mean shear and instantaneous turbulent fluctuations) and particle properties (inertia). In particular, it remains unclear how the different dispersion dynamics affects the statistical behavior of $\langle d^2(t)\rangle$. To gain further insight into this issue, we analyze the probability density function (PDF) of single-particle position for both tracers and inertial particles conditioned to the location of the release plane. This quantity is equivalent to a normalized instantaneous number density distribution of tracers/particles along the wall-normal coordinate.

The PDFs obtained for tracers/particles released very near the wall are reported in Fig. 8 and show that tracers can diffuse toward the outer flow faster than inertial particles in the short period (see Fig. 8(a), computed one crossing time upon injection). Even though the tail of the PDF is characterized by rather small absolute values, it can already be inferred that tracer pairs are more likely to reach spatial regions where differences in the mean streamwise velocity of the fluid are smaller (weak shear): as a result, the velocities of these pairs remain more correlated than the others in time, and relative dispersion is delayed compared to inertial particles which sample near-wall regions of large streamwise fluid velocity (strong shear) longer. At large times (see Fig. 8(b)), all velocity components exhibit a trend of rather steady de-correlation with time and the velocity increments of both tracers and particles eventually thermalize approaching those of the underlying fluid.[32,50] Inertial effects, however, modulate this tendency by generating different distribution profiles: after eight crossing times, particles are seen to accumulate more efficiently than tracers at both channel walls thus sampling more often regions of the flow where shear characteristics favor relative separation. These observations provide already a first interesting insight into the behavior shown in Fig. 7(b).

The PDFs obtained for tracers/particles released at the channel centerline are shown in Fig. 9 for the same time instants considered in Fig. 8. From a qualitative viewpoint the PDF behavior is similar to that observed examining Fig. 8, since it is again driven by local particles-turbulence interactions and modulated by inertial effects: tracers spread in the cross-stream directions faster than particles at small times (Fig. 9(a)); whereas particles accumulate near the wall more than tracers at large times (Fig. 9(b)). Based on this different evolution it can be concluded that (i) in the short period, tracers are more likely than particles to reach regions where shear can boost their pair separation along the streamwise direction: this would justify the different values of $\langle d^2(t)\rangle$ observed for tracers

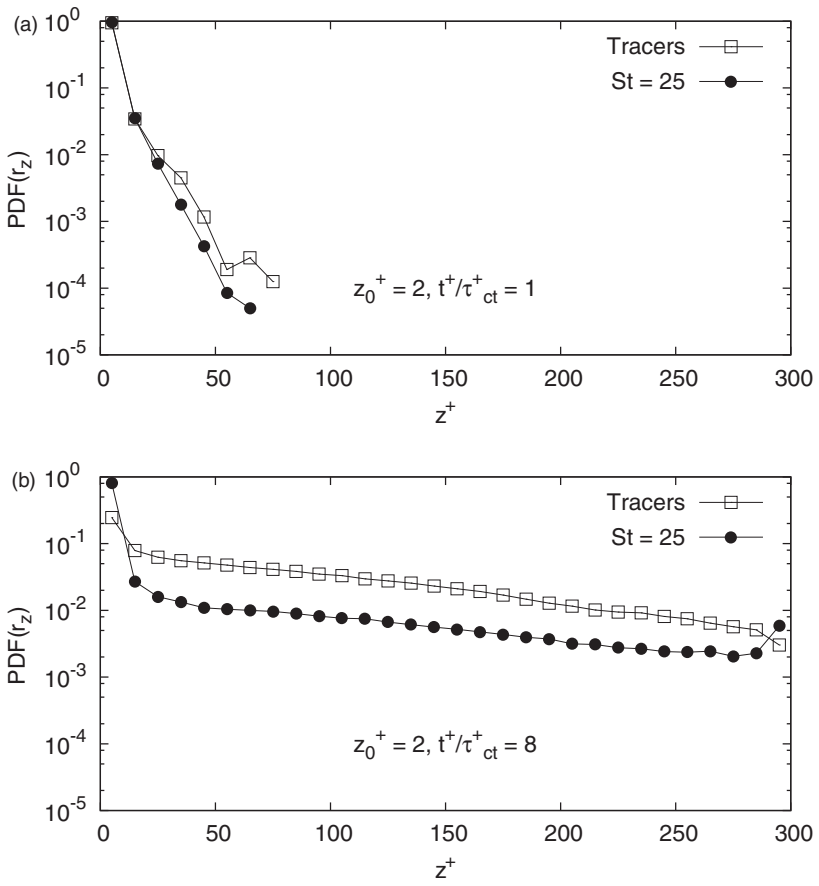

FIG. 8. PDF of single-particle position for tracers (□) and for $St = 25$ particles (•) released from the near-wall $z_0^+ = 2$ plane. Panels: (a) PDF at time $t^+/\tau_{ct}^+ = 1$ and (b) PDF at time $t^+/\tau_{ct}^+ = 8$.

and particles at $t^+/\tau_{ct}^+ = 1$ in Fig. 7(f) and (ii) in the long period, the same turbulent transport mechanism favors separation of particle pairs more than separation of tracer pairs precisely because near-wall accumulation exposes particles to larger velocity differences: the time persistence of this preferential sampling induced by inertia would determine the cross-over in the profiles of $\langle d^2(t)\rangle$ observed for times larger than $t^+/\tau_{ct}^+ \simeq 4$ in Fig. 7(f).

Figs. 8 and 9 indicate that, with respect to the channel centerline, non-stationary single-particle PDFs are symmetrical and Gaussian only for tracers/particles released in the wall-parallel centerplane and only within the time window $0 \leq t^+ \leq 3\tau_{ct}^+$ (as demonstrated, for instance, in Fig. 9(a), which shows the good agreement between the computed PDFs and the Gaussian PDFs). In this case, it is straightforward to derive a parametric model to predict the time evolution of the PDF and a time-dependent law for the variance σ^2 of the distribution. A different parameterization is required when tracers/particles are released in the near-wall region. Based on the evolution of the tails of the PDFs observed in Fig. 8, it seems reasonable to adopt an exponential fitting function of the form $f(\mathcal{T}) = k \cdot \exp(-\mathcal{T}/T)$ where it is set $\mathcal{T} = t^+/\tau_{ct}^+$ to alleviate notation. This function allows data fitting over a larger time range $1 \leq \mathcal{T} \leq 8$. Results obtained upon fitting the numerically obtained, time-dependent values of σ^2, k, and $1/T$ are shown Fig. 10. For ease of discussion, we limit ourselves to inertial particles, yet we consider all Stokes numbers to emphasize the role of inertia. Fig. 10(a) shows fitting of σ^2 with a parabolic function of the form $g(\mathcal{T}) = \alpha\mathcal{T}^2 + \beta\mathcal{T}$. Asymptotic agreement between numerical results (symbols) and parametric model predictions (lines) is very good for each Stokes number, provided that values for α and β are properly set. Note that α decreases (resp. β increases) for increasing St. Figs. 10(b) and 10(c) show fitting of k and $1/T$, respectively, with a function of the form $h(\mathcal{T}) = \gamma + \alpha \cdot \exp(-\mathcal{T}/\beta)$. Again, agreement at large times is generally quite

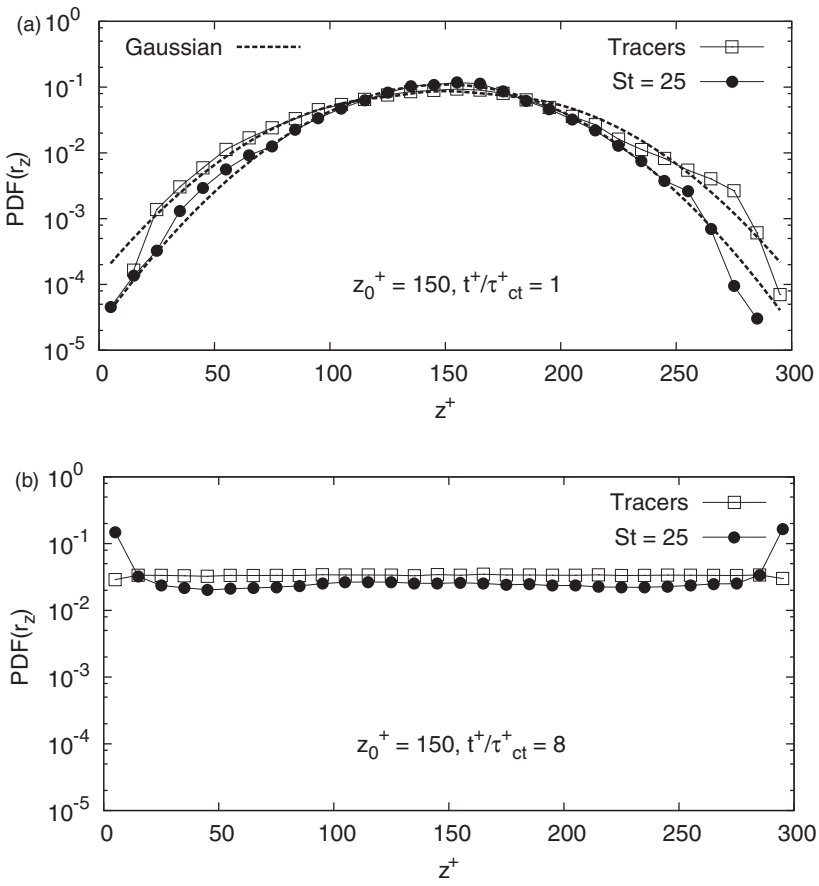

FIG. 9. PDF of single-particle position for tracers (□) and for $St = 25$ particles (•) released from the centerline $z_0^+ = 150$ plane. Panels: (a) PDF at time $t^+/\tau_{ct}^+ = 1$ and (b) PDF at time $t^+/\tau_{ct}^+ = 8$. The dashed lines in panel (a) represent the Gaussian PDF for tracers and for $St = 25$ particles: departure from symmetry close to walls is within the accuracy and convergence limit of the statistics.

good whereas discrepancies arise for the short-term ($t^+/\tau_{ct}^+ < 3$) prediction of k in the $St = 5$ and $St = 25$ cases. These parameterized formulations can be of interest from the perspective of modelling the relative spread of the cloud generated by particles upon release into the flow, a key information when dealing with Lagrangian stochastic simulations of lateral dispersion and mixing phenomena.

C. Number-density distributions of pair separation distance

The single-particle PDFs just discussed represent a straightforward tool for extracting Lagrangian information about the collective dispersion dynamics of tracer/particle swarms. Besides corroborating the qualitative behavior shown in Fig. 5, they provide a plausible explanation to the strong departure of inertial particles from tracer statistics. However, they cannot be used to assess the statistical bias introduced in fixed-time observables like $\langle d^2(t)\rangle$ as a consequence of the simultaneous occurrence of different dispersion regimes (pictured on a qualitative basis in Fig. 4). To investigate on this problem, we propose to examine the number density distributions of the pair separation distance $d(t)$ and of the streamwise component of the pair velocity difference $\delta u_{p,x}(t)$, shown in Figs. 11 and 12 for the same two reference release planes selected in previous figures: $z_0^+ = 2$ and $z_0^+ = 150$, respectively. In these two figures, N_p is the number of pairs characterized by a certain non-dimensional value of $d(t)$ or $\delta u_{p,x}(t)$ that were counted at a given time instant ($t^+/\tau_{ct}^+ = 1$ or 8). Fig. 11(a) shows the different range of separations $d(t)$ sampled by pairs of tracers and pairs of inertial particles after one crossing time upon injection from the $z_0^+ = 2$ plane. Even though

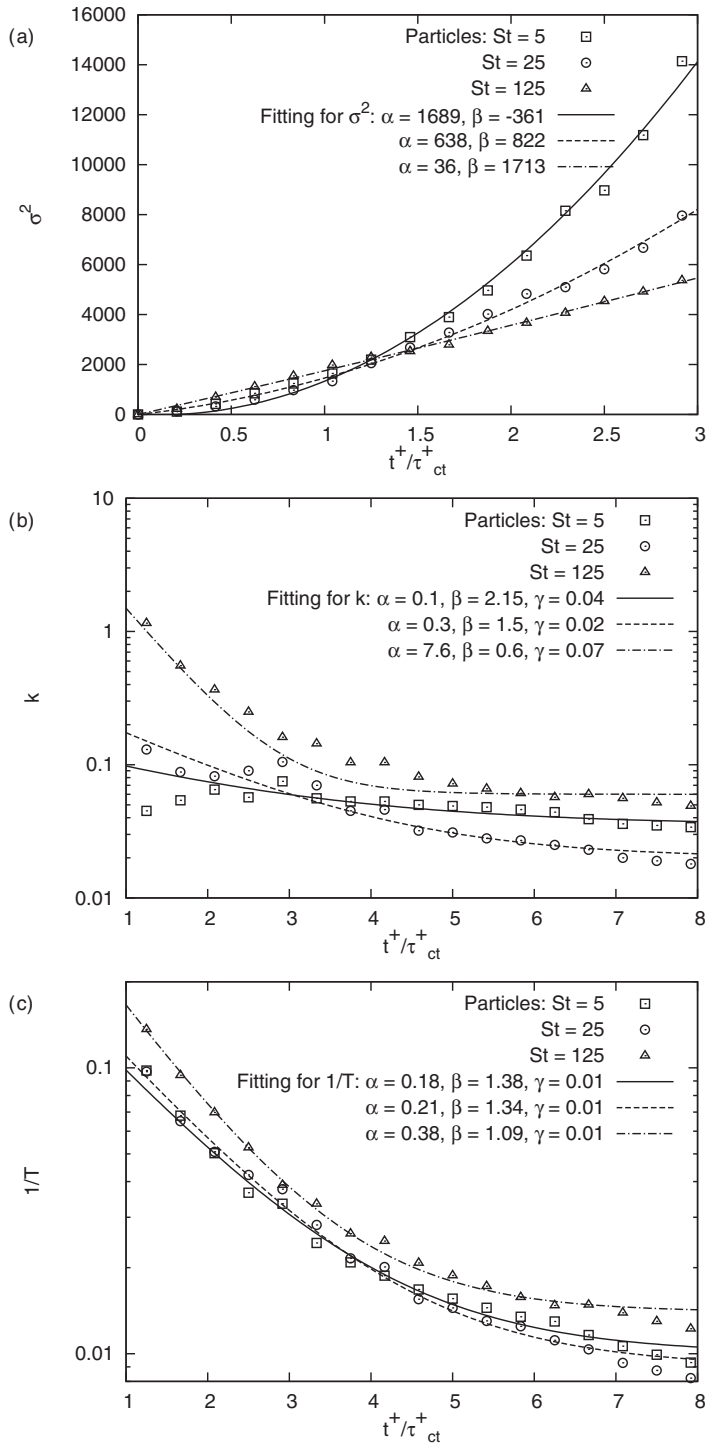

FIG. 10. Parameterized formulations to predict the time evolution of non-stationary single-particle PDFs: (a) fit-parameters for the variance σ^2 of a Gaussian PDF, valid for pairs released from the channel centerline ($z_0^+ = 150$); (b) and (c) fit-parameters for a non-Gaussian exponential PDF, valid for pairs released from the near-wall region ($z_0^+ = 2$).

tracers can escape more easily from the near-wall region (see Fig. 8 and relative discussion), they are observed to cover a narrower range of separations compared to inertial particles. The peak of the N_p distribution for tracers corresponds to a value of $d(t)$ very close to the initial pair separation d_0, whereas the peak of N_p for particles is reached for values of $d(t)$ that are nearly one order

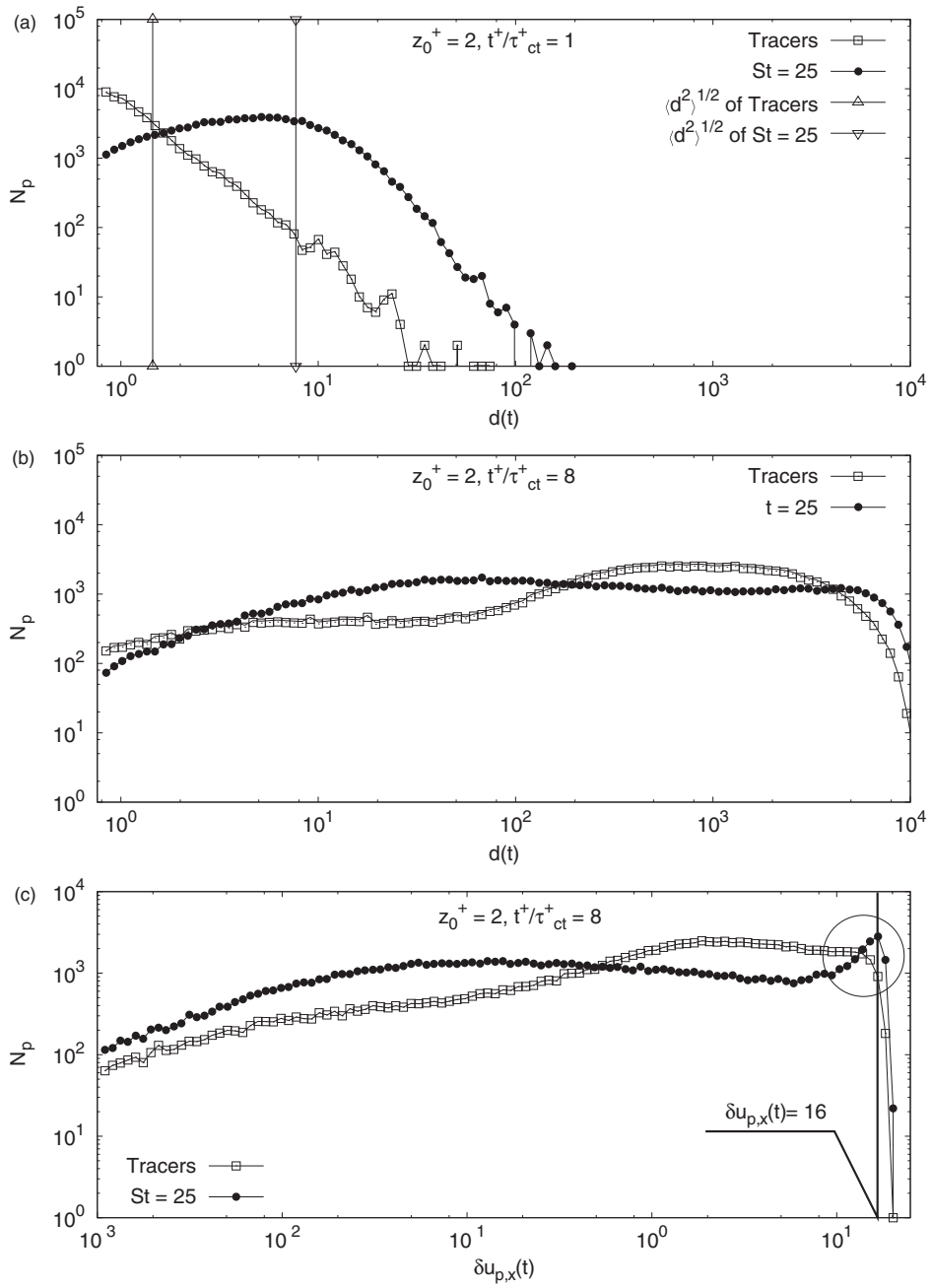

FIG. 11. Number density distribution of pairs N_p as a function of pair separation $d(t)$ (a) and (b) and of longitudinal pair velocity of separation $\delta u_{p,x}$ (c). Both tracer pairs (□) and $St = 25$ particle pairs (•) are considered. Distributions refer to particles released from the near-wall $z_0{}^+ = 2$ plane with initial separation vector oriented in the streamwise direction.

of magnitude larger. Note that the area covered under the N_p curve is also larger for the $St = 25$ particles. The different shape and spread of the two distributions are further quantified by their mean value, given by the square root of $\langle d^2(t = \tau_{ct}) \rangle$ and represented by the vertical lines in Fig. 11(a). The point of interest in interpreting the results just discussed is that, already at relatively short times, the interplay between inertia and turbulence can trigger particle pair separation more efficiently than tracer pair separation thus explaining the different values of $\langle d^2(t) \rangle$ observed in Fig. 7(a).

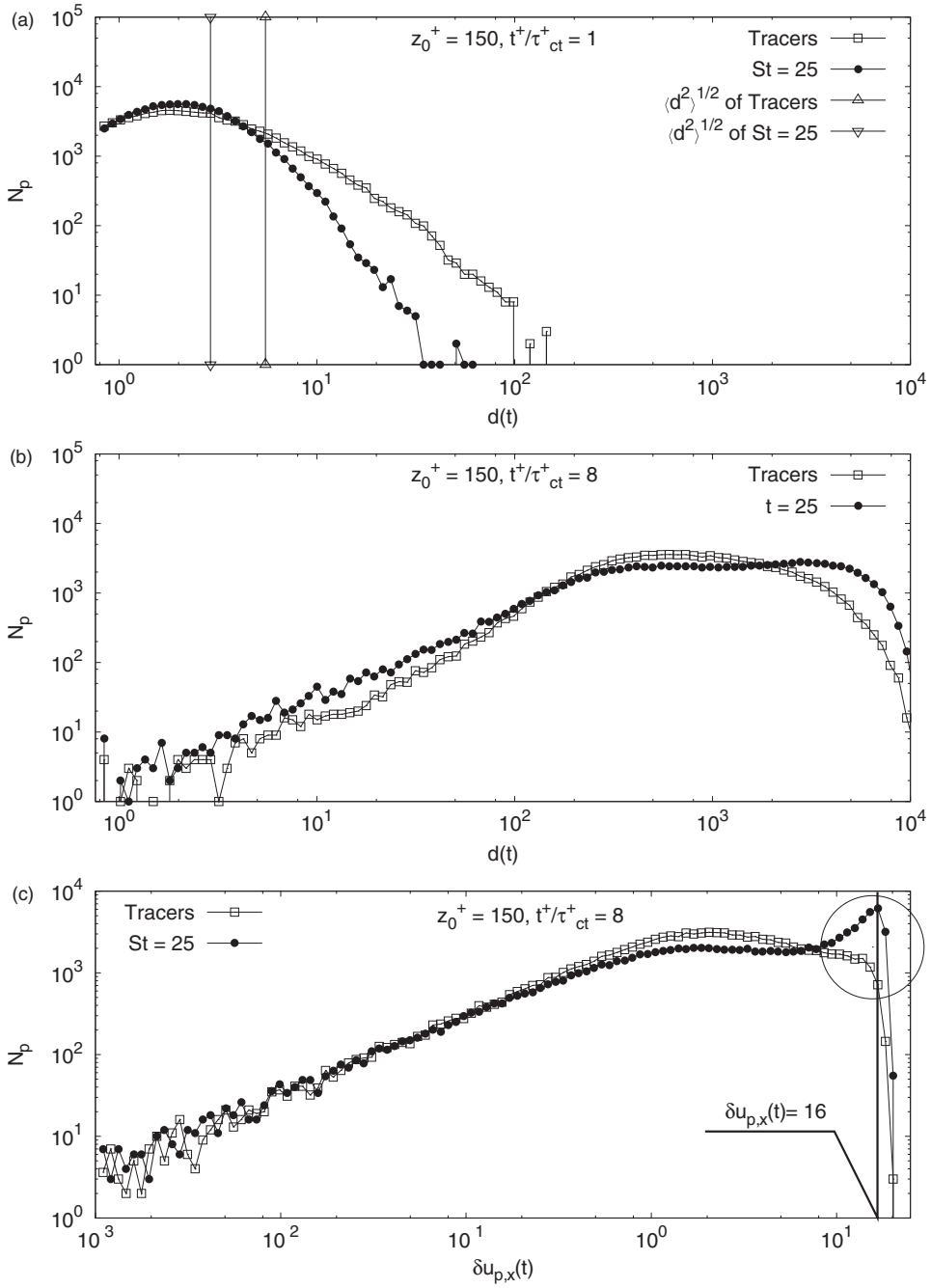

FIG. 12. Number density distribution of pairs N_p as a function of pair separation $d(t)$ (a) and (b) and of longitudinal pair velocity of separation $\delta u_{p,x}$ (c). Both tracer pairs (□) and $St = 25$ particle pairs (•) are considered. Distributions refer to pairs released from the centerline $z_0^+ = 150$ plane with initial separation vector oriented in the streamwise direction.

At long travel times ($t^+/\tau^+_{ct} = 8$), the distribution profiles of Fig. 11(a) evolve becoming those shown in Fig. 11(b). Both profiles level off and, before approaching saturation levels, develop a plateau (wider for particles) at large scales of separation. The area covered under the N_p curves is approximately equal, in agreement with the asymptotic behavior of $\langle d^2(t) \rangle$ shown in Fig. 7(c). An important information that can be extracted from combined examination of Figs. 11(a) and 11(b) is that both tracers and particles sample rather homogeneously the $d(t)$-parameter space with the

consequence that Lagrangian pair dispersion statistics in our problem are affected by contamination from all possible scales of separation, and not just by rare, extreme separation events. Finally, in Fig. 11(c) we show the number density distributions of N_p as a function of $\delta u_{p,x}(t)$ at $t^+/\tau_{ct}^+ = 8$. Given the obvious correlation between $d(t)$ and $\delta u_{p,x}(t)$, the shape of the profiles is qualitatively similar to that observed in Fig. 11(b), except for the presence of a peak (highlighted by the circle) in the N_p-curve of the $St = 25$ particles. This peak, which is not observed for tracers, occurs at $\delta u_{p,x}(t) \simeq 16$: in the present flow configuration, such value corresponds to the streamwise velocity difference between a fluid parcel moving at the wall and a fluid parcel moving along the channel centerline. Intuitively, it could thus be associated to a significant proportion of pairs having one particle near the wall and the other close to the channel centerline. This situation would be compatible with the two time- and scale-dependent separation mechanisms envisioned previously (see Sec. III A). First, in order to achieve large inter-particle distances, inertial pairs released near the wall need to be displaced by small-scale turbulent fluctuations along the wall-normal direction, where they can become exposed to large streamwise velocity differences within the viscous sublayer. Then particles redistribute within the channel due to preferential concentration effects and eventually attain the spatial distribution shown in Fig. 8(b). As our results show, this distribution is associated to a wide spectrum of both separations (Fig. 11(b)) and relative velocities (Fig. 11(c)): during the long-term shear-dominated regimes, separations, and relative velocities can arguably be maximized only in correspondence of particular relative positioning of paired particles.

The validity of this interpretation seems to be corroborated by the number density distributions obtained for pairs released from the channel centerplane, shown in Fig. 12. One crossing time after injection, tracers exhibit a stronger tendency to fill large separations compared to inertial particles, whose mutual distance seems to grow at a slower rate due to preferential concentration effects (see Fig. 12(a)). Later in the evolution, number density distributions for $d(t)$ in Fig. 12(b) and for $\delta u_{p,x}(t)$ in Fig. 12(c) resemble qualitatively those of Figs. 11(b) and 11(c), respectively. Consistently, the peak of N_p at $\delta u_{p,x}(t) \simeq 16$ is observed again, suggesting that the asymptotic spatial distribution of pairs is little dependent on their initial location of release.

To complete the analysis of conditional statistics, in Fig. 13 we show the PDF of the cloud relative spread for both tracers and inertial particles. The spread is evaluated considering the position of the center of mass, R_z, of each pair with respect to the solid wall using a fixed-scale/fixed-velocity type of approach. More specifically, in Fig. 13(a) we show the wall-normal number density distribution of R_z obtained recording the value of R_z whenever a pair is found to meet the threshold condition $d = 1000$, d being the separation distance of that pair in wall units. In Fig. 13(b), the R_z distribution is shown when the threshold condition is applied to the streamwise component of the relative pair velocity ($\delta u_{p,x} = 10$ in wall units). Both figures refer to tracer/particle pairs initially oriented with the mean flow and released either at the $z^+ = 2$ plane or at the $z^+ = 150$ plane. As expected, distributions are always symmetric with respect to the channel centerline when pair injection occurs at $z^+ = 150$, this being true for both tracers (open squares) and inertial particles (black squares) regardless of the threshold condition to be satisfied. Symmetry is of course lost when pair injection occurs at $z^+ = 2$ (see open circles for tracers and black circles for particles) because threshold conditions are matched before a significant proportion of pairs can sample the opposite half of the channel. The interesting feature common to both panels of Fig. 13, however, is that all profiles develop a peak within 50 wall units from the wall. This peak is clearly produced by pairs that sample non-homogeneously the flow domain, namely by a preferential tracer/particle distribution around the instantaneous centre of mass of the pair.

Results of Fig. 13 should be read in connection with results of Figs. 11 and 12. For instance, if one considers the $PDF(R_z)$-profile for the $St = 25$ particles belonging to pairs released from the $z^+ = 2$ plane (black circles in Fig. 13(b)), then one observes that this profile develops a peak around $z^+ \simeq 20$ or, equivalently, that the majority of pairs with $\delta u_{p,x} > 10$ (which produce the peak of N_p around $\delta u_{p,x} \simeq 16$ in Fig. 12(c)) are confined in a near-wall region about 40 wall units thick. Here, paired particles can attain such large relative velocities (and in turn large relative separations, see Fig. 12(b)) only if they are positioned at the far ends of the region where mean shear separation effects can be maximized.

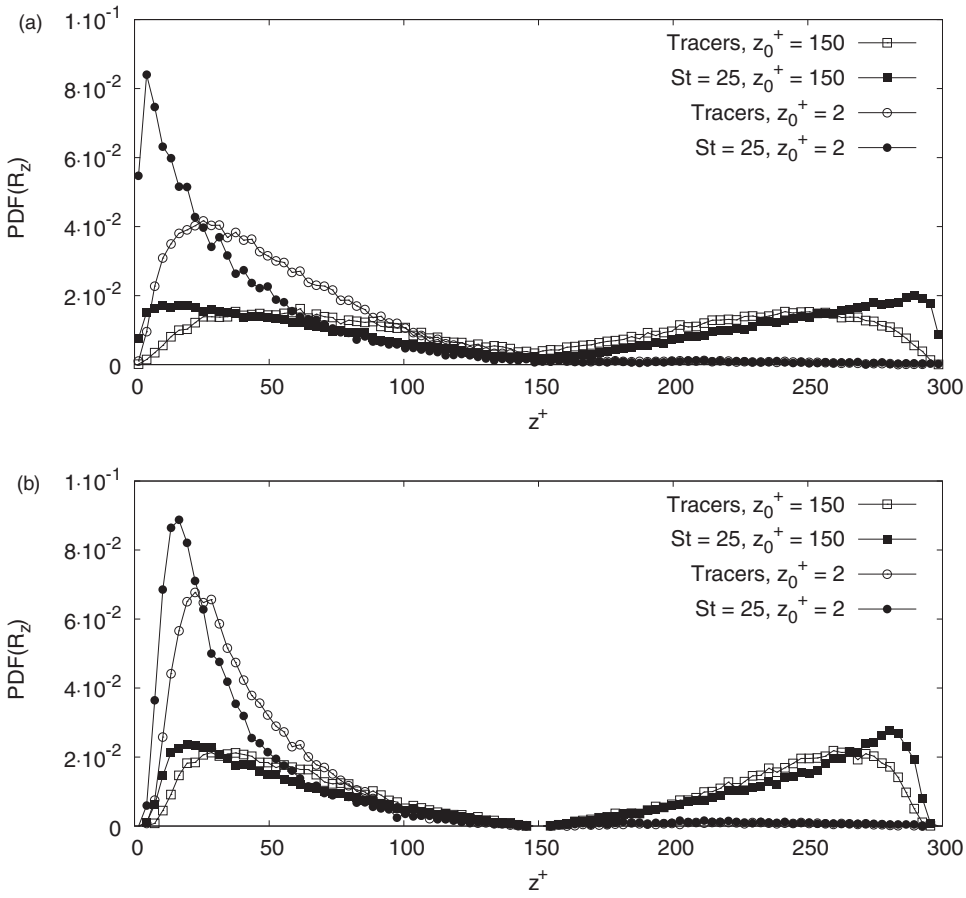

FIG. 13. PDF of the position of the pairs center of mass (a) when pair separation reaches the threshold value $d = 1000$ and (b) when the streamwise relative velocity of the pair reaches the threshold value $\delta u_{p,x}(t) = 10$. Results are shown only for pairs initially oriented along the streamwise direction.

D. Analysis of shear separation effects

For modelling purposes it is important to determine how the dynamics of pair separation has different characteristics in each flow direction due to the presence of shear in the mean velocity field. Most of previous analyses focus on effects of linear shear.[34,50] In this study, we consider nonlinear shear, which is typical of complex non-homogeneous flows in real applications. In sheared flows, pair dispersion is determined by the interplay between shear effects and turbulence effects: currently, it is not clear to what extent these effects can be modelled as separate superimposed phenomena, even in the case of large scale separation. To examine in detail the relative importance of the two phenomena, in this section we isolate shear separation effects from turbulence-induced separation effects by looking at the time evolution of the mean-square separation, $\langle d^2(t)\rangle$, in the absence of unidirectional convection driven by the mean speed of the flow. The idea is to discard the effects of mean velocity gradients and single out those that can be attributed solely to turbulent velocity fluctuations. This is accomplished by re-tracking particles using just the fluctuating streamwise fluid velocity, $u'_{@p}(\mathbf{x_p}, t) = u_{@p}(\mathbf{x_p}, t) - \overline{u}_{@p}(z_p, t)$ with $\overline{u}_{@p}(z_p, t)$ the mean velocity at the wall-normal particle location z_p, in the particle equation of motion. Results of this analysis are presented in Figs. 14 and 15. Lines and symbols in these two figures are the same as in Figs. 6 and 7, respectively. General observations that can be made upon examination of the different profiles in Figs. 14 and 15 and upon comparison against Figs. 6 and 7, respectively, are as follows: (i) Separation is not much affected by shear during the initial dispersion transient in which pair dynamics is dominated by turbulence (one or two crossing times depending on inertia and initial pair orientation). (ii) Separation rates grow

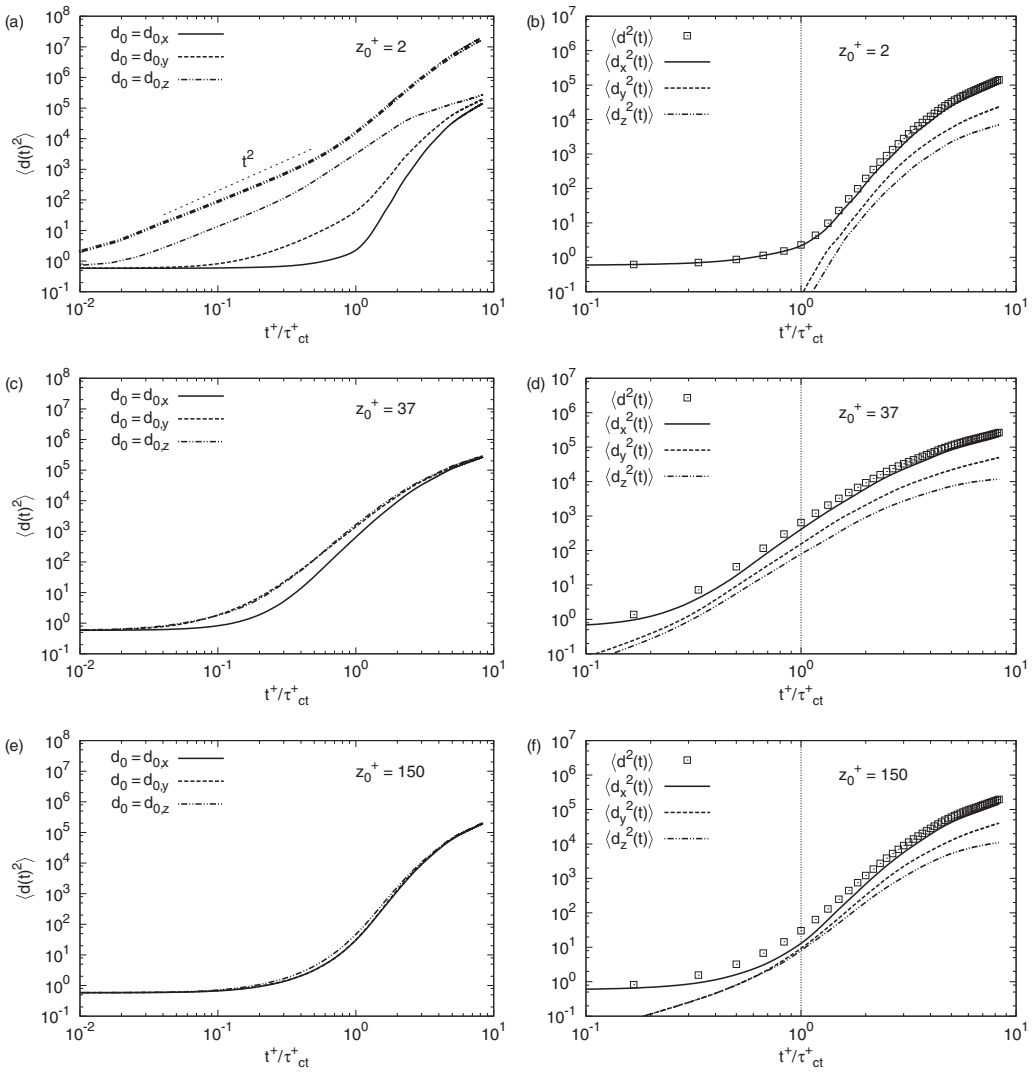

FIG. 14. Time evolution of the mean-square separation, $\langle d^2(t) \rangle$, for tracer pairs in the absence of shear separation effects. Left panels: Behavior of $\langle d^2(t) \rangle$ for pairs with initial separation vector oriented in the streamwise ($d_0 = d_{0,x}$), spanwise ($d_0 = d_{0,y}$), and wall-normal ($d_0 = d_{0,z}$) directions, respectively. Right panels: Behavior of the components of $\langle d^2(t) \rangle$ for pairs with initial separation vector oriented in the streamwise direction. Statistics are shown for three release planes: $z_0^+ = 2$ (a) and (b), $z_0^+ = 37$ (c) and (d), and $z_0^+ = 150$ (e) and (f).

more rapidly when pairs are subject to the action of mean velocity gradients, leading to much higher pair separations at the end of the simulation (the increase being of one/two orders of magnitude roughly, depending again on inertia and initial pair orientation). Not surprisingly, the most evident changes are observed in the near-wall region and particularly for the time evolution of $\langle d^2(t) \rangle$ for pairs initially separated along the wall-normal direction ($d_0 = d_{0,z}$), shown in Fig. 14(a) in the cases with (thick dashed-dotted-dotted line) and without (thin dashed-dotted-dotted line) mean shear. (iii) The streamwise component of $\langle d^2(t) \rangle$ is the dominant one even in the absence of mean shear effects, while the spanwise and wall-normal components do not change, as can be seen comparing panels (b), (d), and (f) of Fig. 14 with panels (b), (d), and (f) of Fig. 6. This is probably due to the fact that streamwise turbulent fluctuations are generally significantly stronger than spanwise and wall-normal fluctuations (especially in the near-wall region). (iv) Without shear, pair separation for both inertial particles and tracers show the same long-term (asymptotic) behavior and is characterized by the

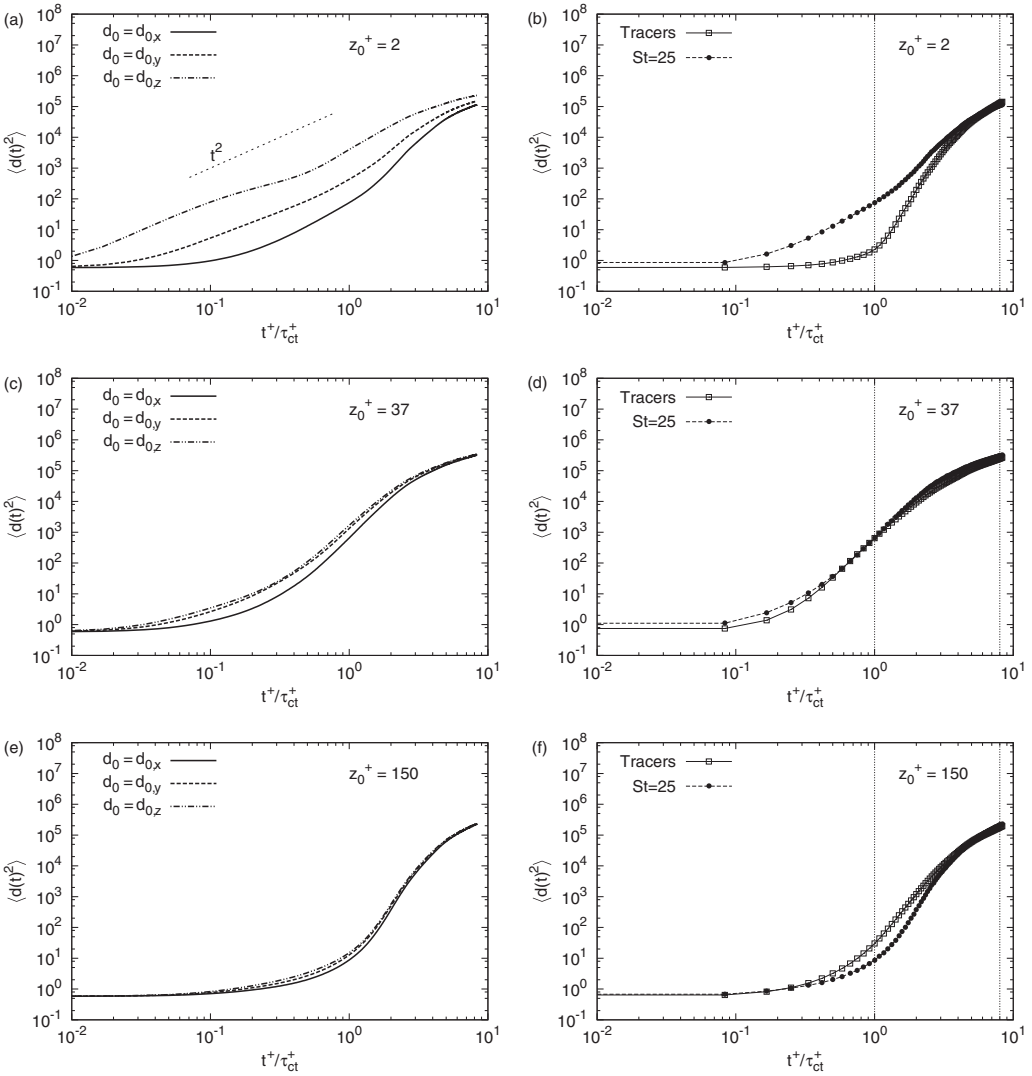

FIG. 15. Time evolution of the mean-square separation for inertial ($St = 25$) particle pairs in the absence of shear separation effects. Left panels: Behavior of $\langle d^2(t) \rangle$ for pairs with initial separation vector oriented in the streamwise ($d_0 = d_{0,x}$), spanwise ($d_0 = d_{0,y}$), and wall-normal ($d_0 = d_{0,z}$) directions, respectively. Right panels: Comparison between time-evolving $\langle d^2(t) \rangle$ for tracers and for inertial ($St = 25$) particles for pairs with initial separation vector oriented in the streamwise direction. Statistics are shown for three release planes: $z_0{}^+ = 2$ (a) and (b), $z_0{}^+ = 37$ (c) and (d), and $z_0{}^+ = 150$ (e) and (f).

same growth rate (see Figs. 15(b), 15(d), and 15(f)). With shear, separation of paired particles grows at a much faster rate than tracers as time elapses (see Figs. 7(b), 7(d), and 7(f)).

IV. CONCLUSIONS AND FUTURE DEVELOPMENTS

In this work, we have examined from a statistical point of view turbulent pair dispersion in non-homogeneous anisotropic shear flow. Statistical characterization of pair dispersion dynamics is of fundamental importance for transport processes in turbulence, particularly those involving mixing of liquids and gasses, since relative separation of pairs is intimately connected to local concentration fluctuations.[56] Because of this connection, the present study is also useful as benchmark for validation of two-point models[17] for predicting the relative velocity distribution of particle pairs in wall-bounded flows. Development of these models will be particularly useful to advance Eulerian approaches to large-eddy simulation (LES) of particle transport in turbulent flows. Current subgrid scale modelling

can have a profound effect on particle dynamics[58] and can affect particle pair dispersion for small initial separations in problems with localized pollutant sources.[59]

Pair dispersion statistics have been analyzed for the reference case of turbulent channel flow, in which the shear profile replicates that of real bounded flows and the structure of the flow exhibits strong anisotropy in the direction normal to the wall. The two-particle statistics that have been considered to probe relative dispersion refer to the classic mean square separation, $\langle d^2(t)\rangle$. The main findings of this study can be summarized as follows:

(i) Turbulent velocity fluctuations and shear dominate pair dispersion at distinct time regimes, giving rise to different anisotropic behaviors. At small timescales, turbulence provides the main mechanism which triggers pair separation. At large times, the effect of mean shear on turbulent fluctuations becomes predominant when the separation distance becomes comparable to the largest scales of the flow. Within this time regime, pair dispersion exhibits a *superdiffusive* nature which is not recovered by standard diffusion laws in a consistent manner and no clear dependency of $\langle d^2(t)\rangle$ with time is noticed. In particular, the Richardson's t^3-scaling behavior is never observed to occur over significantly long time intervals.

(ii) For small initial separation of pairs (smaller than the Kolmogorov length scale), dispersion statistics are strongly influenced by the orientation of the separation vector. In particular, dispersion of pairs oriented along the wall-normal direction appears to be dominated by shear at practically all times.

(iii) The rate at which inertial particles separate can be higher or lower compared to that of fluid tracers depending on the distance from the wall at which pairs are released: the different behavior is determined by the combined influence of inertia and flow anisotropy on pair dynamics. For given inertia, our results indicate that separation rates are higher when pairs are released in the region of maximum Reynolds stress.

(iv) Consistent with the anisotropy of the velocity fluctuations in channel flow, the asymptotic form of the number density distribution for both particles and tracers is significantly non-Gaussian because particle displacements in the different directions are, as a result of mean shear, neither independent nor identically distributed.

(v) When shear separation effects are removed, separation rates appear weakly affected during the initial dispersion transient, but grow slower afterwards leading to much smaller asymptotic separation distances. Even without unidirectional convection, the streamwise component of the separation distance is still the dominant one. However, without shear inertial effects are damped and pair separation shows the same growth rate both for tracers and inertial particles.

These findings represent the first necessary step towards a more thorough comprehension of the physics of pair dispersion in shear flows. The parametric study performed here in the (Re_τ, St) space has been restricted to just one value of the Reynolds number to evaluate inertial effects without changing the degree of turbulence of the flow field. Future extensions of the study should gather a more complete collection of results at several configurations of the system fluid turbulence-inertial particles. In particular, higher values of Re_τ should be considered to investigate the dependence upon the Reynolds number of the inertial particle pair separation.

In view of anisotropy, another issue of considerable interest is the effect of the magnitude of the initial separation vector on pair dispersion statistics. While in this paper we have addressed only the effects associated to different initial pair orientations, looking at changes in the statistics due to changes in the initial pair separation would clearly provide many further information useful for modelling purposes. Finally, inclusion of exit-time statistics (whose computation and evaluation is currently under-way) also represents a future development of this work. A methodology of analysis based on such fixed-scale statistics is expected to provide more clearcut information about scaling behavior of pair separation when averaging at fixed separation scale.

ACKNOWLEDGMENTS

Support from COST Action MP0806 is kindly acknowledged. E.P. gratefully acknowledges the financial contribution from the Erasmus Mundus program of the European Commission.

[1] G. T. Csanady, *Turbulent Diffusion in the Environment*, Geophysics and Atstrophysics Monographs, Vol. 3 (Reidel, 1973), 250 pp.
[2] J. K. Eaton and J. R. Fessler, "Preferential concentration of particles by turbulence," Int. J. Multiphase Flow **20**, 169–209 (1994).
[3] A. Soldati, M. Casal, P. Andreussi, and S. Banerjee, "Lagrangian simulation of turbulent particle dispersion in electrostatic precipitators," AIChE J. **43**, 1403–1413 (1997).
[4] G. Falkovich, A. Fouxon, and M. G. Stepanov, "Acceleration of rain initiation by cloud turbulence," Nature (London) **419**, 151–154 (2002).
[5] R. A. Shaw, "Particle-turbulence interactions in atmospheric clouds," Annu. Rev. Fluid Mech. **35**, 183–227 (2003).
[6] A. Guha, "Transport and deposition of particles in turbulent and laminar flow," Annu. Rev. Fluid Mech. **40**, 311–341 (2008).
[7] A. Soldati and C. Marchioli, "Physics and modelling of turbulent particle deposition and entrainment: Review of a systematic study," Int. J. Multiphase Flow **35**, 827–839 (2009).
[8] F. Toschi and E. Bodenschatz, "Lagrangian properties of particles in turbulence," Annu. Rev. Fluid Mech. **41**, 375–404 (2009).
[9] B. Sawford, "Turbulent relative dispersion," Annu. Rev. Fluid Mech. **33**, 289–317 (2001).
[10] J. H. LaCasce and A. Bower, "Relative dispersion in the sub-surface North Atlantic," J. Mar. Res. **58**, 863–894 (2004).
[11] M. S. Spydell, F. Feddersen, and R. T. Guza, "Observations of drifter dispersion in the surfzone: the effect of sheared alongshore currents," J. Geophys. Res. **114**, C07028, doi:10.1029/2009JC005328 (2009).
[12] P. A. Durbin, "A stochastic model of two-particle dispersion and concentration fluctuations in homogeneous turbulence," J. Fluid Mech. **100**, 279–302 (1980).
[13] J. C. H. Fung and J. C. Vassilicos, "Two-particle dispersion in turbulentlike flows," Phys. Rev. E **57**, 1677–1690 (1998).
[14] J. P. L. C. Salazar and L. R. Collins, "Two-particle dispersion in isotropic turbulent flows," Annu. Rev. Fluid Mech. **41**, 405–32 (2009).
[15] G. Pagnini, "Lagrangian stochastic models for turbulent relative dispersion based on particle pair rotation," J. Fluid Mech. **616**, 357–395 (2008).
[16] L. Biferale, G. Boffetta, A. Celani, B. J. Devenish, A. Lanotte, and F. Toschi, "Lagrangian statistics of particle pairs in homogeneous isotropic turbulence," Phys. Fluids **17**, 115101 (2005).
[17] L. I. Zaichik and V. M. Alipchenkov, "Statistical models for predicting pair dispersion and particle clustering in isotropic turbulence and their applications," New J. Phys. **11**, 103018 (2009).
[18] M. P. Rast and J. F. Pinton, "Pair dispersion in turbulence: the subdominant role of scaling," Phys. Rev. Lett. **107**, 214501 (2011).
[19] M. Picciotto, C. Marchioli, and A. Soldati, "Characterization of near-wall accumulation regions for inertial particles in turbulent boundary layers," Phys. Fluids **17**, 098101 (2005).
[20] A. Aliseda, A. Cartellier, F. Hainaux, and J. C. Lasheras, "Effect of preferential concentration on the settling velocity of heavy particles in homogeneous isotropic turbulence," J. Fluid Mech. **468**, 77–105 (2002).
[21] C. Marchioli and A. Soldati, "Mechanisms for particle transfer and segregation in a turbulent boundary layer," J. Fluid Mech. **468**, 283–315 (2002).
[22] L. R. Collins and A. Keswani, "Reynolds number scaling of particle clustering in turbulent aerosols," New J. Phys. **6**, 119 (1–18) (2004).
[23] J. Chun, D. L. Koch, S. Rani, A. Ahluwalia, and L. R. Collins, "Clustering of aerosol particles in isotropic turbulence," J. Fluid Mech. **536**, 219–251 (2005).
[24] A. Soldati, "Particles turbulence interactions in boundary layers," ZAMM J. Appl. Math. Mech. **85**, 683–699 (2005).
[25] J. Bec, L. Biferale, M. Cencini, A. Lanotte, S. Musacchio, and F. Toschi, "Heavy particle concentration in turbulence at dissipative and inertial scales," Phys. Rev. Lett. **98**, 084502 (2007).
[26] E. Calzavarini, M. Cencini, D. Lohse, and F. Toschi, "Quantifying turbulence-induced segregation of inertial particles," Phys. Rev. Lett. **101**, 084504 (2008).
[27] A. Goto and J. C. Vassilicos, "Sweep-stick mechanism of heavy particle clustering in fluid turbulence," Phys. Rev. Lett. **97**, 054503 (2008).
[28] R. Monchaux, M. Bourgoin, and A. Cartellier, "Preferential concentration of heavy particles: A Voronoi analysis," Phys. Fluids **22**, 103304 (2010).
[29] E. Balkovsky, G. Falkovich, and A. Fouxon, "Intermittent distribution of inertial particles in turbulent flows," Phys. Rev. Lett. **86**, 2790–2793 (2001).
[30] L. I. Zaichik, O. Simonin, and V. M. Alipchenkov, "Two statistical models for predicting collision rates on inertial particles in homogeneous isotropic turbulence," Phys. Fluids **15**, 2995–3005 (2003).
[31] G. Falkovich and A. Pumir, "Intermittent distribution of heavy particles in turbulent flow," Phys. Fluids **16**, L47–L50 (2004).
[32] J. Bec, L. Biferale, A. S. Lanotte, A. Scagliarini, and F. Toschi, "Turbulent pair dispersion of inertial particles," J. Fluid Mech. **645**, 497–528 (2010).
[33] J. Bec, L. Biferale, M. Cencini, A. S. A. Lanotte, and F. Toschi, "Intermittency in the velocity distribution of heavy particles in turbulence," J. Fluid Mech. **646**, 527–536 (2010).
[34] A. Celani, M. Cencini, M. Vergassola, E. Villermaux, and D. Vincenzi, "Shear effects on passive scalar spectra," J. Fluid Mech. **523**, 99–108 (2005).
[35] L. F. Richardson, "Atmospheric diffusion shown on a distance-neighbour graph," Proc. R. Soc. London, Ser. A **110**, 709–737 (1926).
[36] M. S. Spydell and F. Feddersen, "The effect of a non-zero Lagrangian time scale on bounded shear dispersion," J. Fluid Mech. **691**, 69–94 (2012).

[37] C. Marchioli, M. Picciotto, and A. Soldati, "Particle dispersion and wall-dependent turbulent flow scales: implications for local equilibrium models," J. Turbul. **7**(60), 1–12 (2006).
[38] J. H. LaCasce, "Statistics from Lagrangian observations," Prog. Oceanogr. **77**, 1–29 (2008).
[39] G. I. Taylor, "Dispersion of soluble matter in solvent flowing slowly through a tube," Proc. R. Soc. London **219**, 186–203 (1953).
[40] G. I. Taylor, "The dispersion of matter in turbulent flow through a pipe," Proc. R. Soc. London **223**, 446–468 (1954).
[41] R. Aris, "On the dispersion of a solute in a fluid flowing through a tube," Proc. R. Soc. London **235**, 67–77 (1956).
[42] V. L. Schiller and A. Naumann, "Über die grundlegenden Berechnungen bei der Schwerkraftaufbereitung," Ver. Deut. Ing. **77**, 318–320 (1933).
[43] C. Marchioli, A. Soldati, J. G. M. Kuerten, B. Arcen, A. Taniere, G. Goldensoph, K. D. Squires, M. F. Cargnelutti, and L. M. Portela, "Statistics of particle dispersion in direct numerical simulations of wall-bounded turbulence: results of an international collaborative benchmark test," Int. J. Multiphase Flow **34**, 879–893 (2008).
[44] B. Arcen, A. Tanière, and B. Oesterlé, "On the influence of near wall forces in particle-laden channel flows," Int. J. Multiphase Flow **32**, 1326–1339 (2006).
[45] C. Marchioli, M. Picciotto, and A. Soldati, "Influence of gravity and lift on particle velocity statistics and transfer rates in turbulent vertical channel flow," Int. J. Multiphase Flow **33**, 227–251 (2007).
[46] J. W. Deardorff and R. L. Peskin, "Lagrangian statistics from numerically integrated turbulent shear flow," Phys. Fluids **13**, 584–595 (1970).
[47] G. Lacorata, A. Mazzino, and U. Rizza, "3D chaotic model for subgrid turbulent dispersion in large-eddy simulations," J. Atmos. Sci. **65**, 2389–2401 (2008).
[48] G. Boffetta, A. Celani, A. Crisanti, and A. Vulpiani, "Pair dispersion in synthetic fully developed turbulence," Phys. Rev. E **60**, 6734–6741 (1999).
[49] Note that, when $d_0 = d_{0,z}$, $\langle d^2(t)\rangle$ grows as t^2 during the early stages of separation, as predicted by Batchelor's scaling theory the appearance of this *ballistic* regime, which produces a strong transient departure from the Richardson diffusion, indicates that tracers initially separate *as if* the underlying velocity field was frozen (Ref. 32) [please see G. K. Batchelor, "The application of the similarity theory of turbulence to atmospheric diffusion," Q. J. R. Metereol. Soc. **76**, 133–146 (1950) and G. K. Batchelor, "Diffusion in a field of homogeneous turbulence II. The relative motion of particles," Proc. Cambridge Philos. Soc. **48**, 345–362 (1952)].
[50] P. Shen and P. K. Yeung, "Fluid particle dispersion in homogeneous turbulent shear flow," Phys. Fluids **9**, 3472–3484 (1997).
[51] A. El Maihy and F. Nicolleau, "Investigation of the dispersion of heavy-particle pairs and Richardson's law using kinematic simulation," Phys. Rev. E **71**, 046307 (2005).
[52] M. Wilkinson and B. Mehlig, "Caustics in turbulent aerosols," Europhys. Lett. **71**, 186–192 (2005).
[53] J. Kim, P. Moin and R. Moser, "Turbulence statistics in fully developed channel flow at low Reynolds number," J. Fluid Mech. **177**, 133–166 (1987).
[54] The velocity difference between two paired particles P_1 and P_2 is defined as $\delta\mathbf{u}_p(t) = |\mathbf{u}_p^{P_1}(\mathbf{x}_p^{P_1}(t), t) - \mathbf{u}_p^{P_2}(\mathbf{x}_p^{P_2}(t), t)|$.
[55] G. Boffetta and I. M. Sokolov, "Statistics of two-particle dispersion in two-dimensional turbulence," Phys. Fluids **14**, 3224–3232 (2002).
[56] M. Bourgoin, N. T. Ouellette, H. Xu, J. Berg, and E. Bodenschatz, "The role of pair dispersion in turbulent flow," Science **311**, 835–838 (2006).
[57] B. Lüthi, S. Ott, J. Berg, and J. Mann, "Lagrangian multi-particle statistics," J. Turbul. **8**(45), 1–17 (2007).
[58] F. Bianco, S. Chibbaro, C. Marchioli, M. V. Salvetti, and A. Soldati, "Intrinsic filtering errors of Lagrangian particle tracking in LES flow fields," Phys. Fluids **24**, 045103 (2012).
[59] P. K. Yeung, "Lagrangian investigations of turbulence," Annu. Rev. Fluid Mech. **34**, 115–142 (2002).